Tephrostratigraphy of the Late Glacial and Holocene sediments of Puyehue Lake (Southern Volcanic Zone, Chile, 40°S)

Sébastien Bertrand[1,a], Julie Castiaux[1] and Etienne Juvigné[2]

[1] Clays and Paleoclimate Research Unit, University of Liège, Belgium

[2] Geomorphology and Quaternary Geology, University of Liège, Belgium

[a] Present address: Marine Chemistry and Geochemistry, Woods Hole Oceanographic Institution, USA

Correspondence to: S. Bertrand, Marine Chemistry and Geochemistry, Woods Hole Oceanographic Institution, MA 02543, Woods Hole, USA. Tel: +1-508.289.3410, Fax: +1-508.457.2193, E-mail: sbertrand@whoi.edu

Abstract

We document the mineralogical and geochemical composition of tephra layers identified in the late Quaternary sediments of Puyehue Lake (Southern Volcanic Zone of the Andes, Chile, 40°S) to identify the source volcanoes and to present the first tephrostratigraphic model for the region. For the last millennium, we propose a multi-criteria correlation model based on five tephra layers identified at seven coring sites. The two upper tephras are thin fine-grained green layers composed of more than 80% rhyodacitic glass shards, and associated to the AD 1960 and AD 1921-22 eruptions of the Puyehue-Cordon de Caulle volcanic complex. The third tephra is a sandy layer dominated by orthopyroxene, and related to the AD 1907 eruption of Rininahue maar. An olivine-rich tephra was deposited at the end of the 16th century, and a tephra characterized by a two pyroxene association marks the second half of the first millennium AD. In addition, we detail the tephra succession of an 11.22 m long sediment core covering the last 18,000 years. The results demonstrate that the central province of the Southern Volcanic Zone has been active throughout the last deglaciation and the Holocene, with no increase in volcanic activity during glacial unloading.

Keywords

Tephra, Southern Volcanic Zone, lake sediments, South America, Chile

Introduction

The identification and characterization of volcanic layers deposited in continuous sedimentary environments generally provide a detailed history of the past volcanic activity of the study region and allow time correlation of sites across extensive areas (e.g., Juvigné, 1993; Boygle, 1999; Schmidt et al., 2002; Shane et al., 2002; Wulf et al., 2004). Tephrostratigraphy is one of the best tools for correlating long sedimentary records of environmental and climatic changes (e.g., Hodgson et al., 1998; Newnham and Lowe, 1999; Newton and Metcafle, 1999; Litt et al., 2003). Early studies have demonstrated that airfall tephra deposits consist of volcanic glass shards (including pumice), minerals and lithic fragments (e.g., Froggatt, 1992; Ortega-Guerrero and Newton, 1998; Boygle, J., 1999). Although differential settling is responsible for changes in the relative abundance of minerals with distance to the source (Juvigné, 1983, 1993), the composition of the minerals and glass shards occurring in tephra layers remains the best means of correlating tephra layers. In addition, accurately identifying the tephra layers deposited in lake systems is critical because not only are they passive chronological markers, but under certain conditions they are also able to cause ecological changes (Sterken, 2003; Telford et al., 2004).

In south-central Chile, continuous tephrostratigraphic records remain scarce and are restricted to the southernmost part of the country (e.g., Haberle and Lumley, 1998; Kilian et al., 2003; Naranjo and Stern, 2004). Authors generally opted to study the volcanic edifices themselves (Moreno 1977; Gerlach et al., 1988). However, due to the high volcanic activity of the Southern Volcanic Zone, the region has a high potential to provide valuable and continuous tephrostratigraphic and tephrochronological records.

In this paper, we report the first continuous tephra record of south-central Chile (36-42°S), based on the tephra layers identified in the sediment of Puyehue Lake (40°S). Using previously

published age models and historical chronicles, we demonstrate that the mineralogical and geochemical composition of the recent tephras is particularly helpful for correlating recent sediment sequences collected in different sub-basins of Puyehue Lake. In addition, we present the mineralogical and geochemical composition of tephras identified in a continuous 18,000 year-long sedimentary archive and we discuss their potential to provide reliable chronostratigraphic markers for the region.

Study area

Puyehue Lake (40.70°S, 72.45°W) is located at the foot of the Cordillera de Los Andes at an elevation of 185 m.a.s.l. (Fig. 1). It is surrounded by several volcanoes, which all belong to the central petrographic province (37 to 41.5°S) of the currently active Southern Volcanic Zone of Chile (SVZ, 33 to 46°S) (Gerlach et al., 1988; Stern, 1989; López-Escobar et al., 1995). The SVZ results from the subduction of the Nazca plate under the South American plate. While its northern part is characterized by andesitic volcanoes, its southern part is dominated by strato-volcanoes composed of basalts or andesitic basalts with lesser amount of silicic lavas (Lopez-Escobar et al., 1977; Hickey et al., 1984; Lopez-Escobar, 1984). Five volcanoes or volcanic complexes occur within 50 km of Puyehue Lake, and are probably at the origin of most of the tephras deposited in the lake sediments (Fig. 1):

- The Puyehue-Cordon de Caulle volcanic complex (PCCVC, 2236 m.a.s.l.) is located at the northern border of the lake and is composed of a cluster of eruptive centers that extends between the Cordillera Nevada caldera to the northwest and to the Puyehue strato-volcano to the southeast (Gerlach et al., 1988; Lara et al., 2006). Between these two volcanic edifices the Cordon de Caulle fissure system strikes in a northwest-southeast direction (Fig. 1). Since the beginning of its

formation 200,000 years ago, this unusual complex has emitted lavas, tephras and ignimbrites with a composition ranging from basalts to rhyolite. During the growth of PCCVC, the lava composition evolved from basaltic to silicic (Gerlach et al., 1988; Lara et al., 2006). The most recent eruption of Cordon de Caulle occurred in AD 1960, 47 hours after the M 9.5 earthquake of Valdivia. It was characterized by the emission of rhyodacite and rhyolite lavas in addition to pumices. A similar eruption occurred in AD 1921-22 (Lara et al., 2006).

- The Carran-Los Venados volcano group (1114 m.a.s.l.) occupies a low-lying area at the northern part of the PCCVC. It is composed of a group of about 50 scoria cones, maars, and a small stratovolcano that are broadly aligned along a 17 km long ENE-WSW trend. Three historical eruptions have been reported: Rininahue maar (AD 1907-08), Nilahue maar (AD 1955) and Mirador volcano (AD 1979) (Lopez-Escobar and Moreno, 1981).

- The Antillanca volcanic complex occurs at the South-East of Puyehue Lake (Fig. 1). It consists in a late Pleistocene to Holocene basaltic strato-volcano peaking at 1990 m.a.s.l. and multiple post-glacial monogenetic scoria cones (Lopez-Escobar et al., 1995). This complex emitted post glacial and Holocene lavas with a composition ranging from olivine basalt to mafic andesite (Lopez-Escobar et al., 1995). Casablanca volcano (1990 m.a.s.l.) is the highest eruptive monogenetic center of this volcanic complex (González-Ferrán, 1994). No historical eruption of the Antillanca volcanic complex has been recorded (González-Ferrán, 1994).

- The Puntiagudo volcano (2493 m.a.s.l.) is an early Pleistocene strato-volcano of basalt-andesitic composition (González-Ferrán, 1994). Its acute morphology is due to glacial erosion that has not been overlain or destroyed by later volcanic activity. No historical activity has been reported.

- The Osorno volcano (2652 m.a.s.l.) separates lakes Todos Los Santos and Llanquihue. It is a strato-volcano formed during the early Pleistocene and Holocene by basaltic lava and pyroclastic

104 flows. Holocene eruptions are of andesitic or basaltic composition. Its first historical but poorly
105 documented eruption occurred in AD 1575 (González-Ferrán, 1994). In addition, two historical
106 effusive eruptions have been recorded in AD 1790 and in AD 1835 and they are both
107 characterized by the emission of basaltic-andesitic lava (González-Ferrán, 1994).
108
109 The intense activity of the previously mentioned volcanoes since the early Pleistocene is
110 responsible for the volcanic nature of the rocks and soils occurring in the area (Laugenie, 1982;
111 Bertrand and Fagel, 2008). Because this region is affected by intense westerly winds, most of the
112 eruptive products are deposited to the eastern side of regional volcanoes, i.e. close to the
113 Chile/Argentina border (Besoain, 1985; Lara et al., 2006). In consequence, the tephras layers
114 deposited in Puyehue Lake and in other lakes, peat bogs and soils similarly located to the west of
115 the regional volcanoes are relatively thin and do not disturb the continuity of the sedimentary
116 records. In soils and peatbogs, the tephras are generally altered by physical and chemical
117 weathering processes (Laugenie, 1982; Hodder et al., 1991; Kilian et al., 2003; Bertrand and
118 Fagel, 2008), and are therefore not ideal for detailed tephrostratigraphic correlations. Tephra
119 layers deposited in lake sediments are however generally well preserved, especially in lakes
120 characterized by high sedimentation rates and absence of bioturbation (de Fontaine et al., 2007),
121 such as Puyehue. The tephra layers deposited in Puyehue Lake are therefore very promising in
122 terms of stratigraphic correlation between sedimentary archives collected for paleoclimatic and/or
123 paleoenvironmental purposes.
124
125 **Material and analytical methods**
126
127 *Material*

The results presented in this paper were obtained on different sediment cores collected during a coring campaign of Puyehue Lake in 2001-2002 (De Batist et al., 2008):

- Two short gravity (pilot) cores (PU-I-P1 and PU-II-P2) taken at coring sites PU-I and PU-II, which were selected from a preliminary geophysical investigation of the lake sedimentary infill (Charlet et al., 2008; Figs. 1 and 2)
- Five short gravity cores (PU-SC1/2/3/4/7) collected at diverse locations in the eastern part of the lake (see location in Fig. 2)
- A continuous 11.22 m long piston core collected at PU-II site (40°41.843'S, 72°25.341'W), which is located on a sublacustrine moraine ridge at 48.4 m depth.

The seven short cores are composed of homogenous to laminated silty sediments that are detailed in Bertrand et al. (2005) (Fig. 2). They contain black tephra layers, pumice layers and organic-rich sand layers. Likewise, PU-II long core is composed of homogeneous to finely laminated silty sediments (Bertrand et al., 2008) and it contains 78 sandy layers with a thickness ranging from 1 to 75 mm (Fig. 3). These layers are supposed to be tephras in original position and are distinguished from the host sediment by several characteristics: coarser grain-size, darker or distinct color and sharp lower and upper limits.

Sampling

The tephras occurring in the short gravity cores PU-I-P1 and PU-II-P2 were carefully sampled avoiding under- and overlying host sediment. On the other hand, the long and short sediment cores were sampled in 1-cm thick slices and the samples containing tephras were

152 selected for analysis. The grain-size distributions of the tephra deposits (Fig. 4) demonstrate that
153 the tephra material frequently contains host sediment originating from percolation between coarse
154 tephra particles. Therefore, samples were sieved at 75 µm, where the limit between the host
155 sediment and the tephra particles seems to be the most appropriate to discard most of the host
156 sediment particles. Moreover, this sieving step also discards most of the host sediment that is
157 usually found in addition to tephra particles in the 1 cm thick sediment slices. Finally, to avoid
158 the presence of coarse grains in smear slides, samples were sieved at 420 µm and the sole 75-420
159 µm fraction was investigated. Tephras are labeled according to their mid depth rounded to the
160 closest unit (e.g., tephra at 102.3–109.8 cm in PU-II core is labeled PU-II-106).
161
162 For PU-II long core, preliminary investigations have shown that aliquots containing tephra
163 layers thinner than 6 mm were inappropriate for accurate tephra investigations. Therefore, only
164 the 15 thickest tephra layers (> 6 mm) were selected for analysis. These tephras are well
165 distributed throughout the core (Fig. 3).
166
167 *Mineralogical determination*
168
169 All the samples were treated with H_2O_2, $HCl_{10\%}$ and Aqua $Regia_{50\%}$, and two smear slides of
170 this cleaned material were mounted for investigations under (1) binocular lens and (2) polarizing
171 microscope. In addition, heavy minerals were separated in bromoform (density 2.8) using
172 centrifugation and their nature was determined under a polarizing microscope. Between 105 and
173 176 grains were counted in each smear slide. In both cases, the grains were grouped in different
174 populations, and the data are presented in Supplementary Tables 1 and 2.
175

176 *Geochemical analyses*

177

178 Because the geochemistry of the glass shards reflects the composition of the magma at the time
179 of eruption of the tephra (Ortega-Guerrero and Newton, 1998), the glass shards of the glass-rich
180 tephra layers were separated and analyzed for major elements by electron microprobe. Glass
181 shards were hand-picked in the 75-420 um fraction and mounted on a petrographic slide using
182 epoxy resin. The grain mounts were then polished to a flat, smooth surface with a 1 μm
183 polycrystalline diamond paste on an automated polishing wheel (Struers DP-U2). The data were
184 obtained on a Cameca SX50 microprobe following the recommendations of Hunt & Hill (1993).
185 Ten elements were analyzed (Na, Mg, Si, Al, Fe, Ca, Ti, K, Cr, Mn) using the following
186 instrumental conditions: accelerating voltage 15 kV and beam current 6 nA. A highly defocused
187 beam (beam diameter: 25 μm) was used to prevent volatilization of alkalis from the glass.
188 Sodium, potassium and silicon were analyzed first in order to obtain the best possible accuracy
189 for these elements. The standards and counting times used for each element are given in Table 1.
190 Geochemical data were normalized to 100% to correct for varying degrees of hydratation (3.9 ±
191 1.1 %) and to enable the comparison of our results to data obtained with different electron
192 microprobes and under different instrument conditions (Froggatt, 1992). The reported means are
193 averages of analyses made on multiple discrete shards from each tephra layer (see Supplementary
194 Table 3). Between 9 and 15 glass shards were analyzed per tephra. Petrological classification is
195 based on the Total Alkali–Silica diagram (Le Bas et al., 1986). Similar analyses were conducted
196 on plagioclases picked in two key tephra layers (PU-II-P2-11 and PU-I-P1-54).
197 We used the similarity coefficient (SC) of Borchardt et al. (1972) as an objective and quantitative
198 basis for correlating tephras using the geochemical data obtained on the tephras of the two pilot

199 cores (PU-II-P2 and PU-I-P1). A value of 1.00 represents a perfect match. Values ≥ 0.92 are
200 generally taken as indicative of correlation between tephra samples (Froggatt, 1992).
201
202 *Grain-size*
203
204 The grain-size distributions were obtained by a combination of laser particle sizing and sieving
205 according to the following method. Samples were wet sieved at 420 μm and the two fractions
206 were subsequently freeze-dried and weighted with a 3 decimal precision (10^{-3} g). The coarser
207 than 420 μm fraction was analyzed by dry sieving at half ϕ intervals while the finer than 420 μm
208 fraction was analyzed by laser diffraction on a Malvern Mastersizer 2000 particle analyzer. The
209 grain-size data obtained by both methods were then merged by using the dry weights of each
210 grain-size class, and the statistical parameters were calculated using the GRADISTAT software
211 (Blott and Pye, 2001).
212
213 *Chronology*
214
215 The age of the historical tephras identified in pilot cores PU-I-P1 and PU-II-P2 was assessed
216 by comparing age models based on radionuclides (^{210}Pb and ^{137}Cs — Arnaud et al., 2006) and
217 varve-counting (Boës and Fagel, 2008) to historical chronicles and AMS radiocarbon dates. For
218 PU-II long core, the ages are derived from an age model based on 9 AMS radiocarbon dates
219 calibrated with BCal using atmospheric data of Stuiver et al. (1998) (Bertrand et al., 2008).
220
221 **Results and discussion**

222

223 *Historical tephras (Fig. 2)*

224

225 *Description of tephras occurring in recent sediments*

226 a. Core PU-II-P2

227 Four tephra layers occur in pilot core PU-II-P2:

228 - **PU-II-P2-4** is macroscopically described as a 5 mm thick light green and fine-grained layer
229 (dust and fine ash). Its bulk mineralogical composition is dominated by colorless and vesiculated
230 glass shards of rhyodacitic composition (Fig. 5a). The glass shards represent more than 80% of
231 the bulk fraction and the remaining grains probably originate from the host sediment, as
232 demonstrated by the occurrence of diatoms intercalated between the tephra particles.

233

234 - **PU-II-P2-8** is a 5 mm thick light grey layer that essentially consists in colorless vesiculated
235 glass shards of rhyodacitic composition (Fig. 5b). Its grain-size is characteristic for dust and fine
236 ash. As for PU-II-P2-4 tephra, its bulk composition is dominated (80%) by glass shards.

237

238 - **PU-II-P2-11** is a 4 mm thick black sandy layer. Its bulk mineralogical composition is
239 characterized by a high amount of phenocrystals (57%) together with semi-opaque scoriae
240 including crystals (27%), opaque minerals (12%) and colorless to brownish transparent
241 vesiculated glass shards (3%). The phenocrystals are dominated by basic feldspars (Fig. 6), which
242 are coated by rhyodacitic and highly vesiculated glass (Fig. 5c). The rare glass shards are highly
243 vesiculated and their chemical composition ranges from dacite to rhyolite. The mafic suite is
244 dominated by orthopyroxene (83%, hypersthene), occurring in association with clinopyroxene
245 (13%, augite) and dark brown amphibole (2.4%, tchermakite). The most striking characteristics

246 of this tephra are the abundance of phenocrystals and the co-occurrence of basic feldspars and
247 massive rhyolitic glass coating.
248
249 - **PU-II-P2-42** is a 5 mm thick black sand layer. Its bulk mineralogy is characterized by (1)
250 opaque to partly translucent scoriae (59%); (2) brownish glass shards (25% massive and 3%
251 vesiculated) including numerous automorphic microcrystals and (3) crystals (8% felsic and 2%
252 mafic). The heavy mineral suite is dominated by olivine (77%), which occurs together with
253 orthopyroxene (11%) and clinopyroxene (8%). The chemical composition of the brownish glass
254 shards corresponds to a basaltic andesite (Fig. 5d).
255
256 b. Core PU-I-P1
257 The sediment core PU-I-P1 contains two tephra layers:
258 - **PU-I-P1-48** is a 5 mm thick layer of pumice lapilli and colorless highly vesiculated glass shards
259 (dust and fine ash) of rhyodacitic composition (Fig. 5e) overlain by a 35 mm layer of silty light
260 gray particles. The presence of non volcanic minerals (tourmaline, zircon) and diatoms in the
261 bulk sample suggests that the upper part of this tephra may have been reworked.
262
263 - **PU-I-P1-54** consists in a 5 mm thick black sand layer bearing the following characteristics: (1)
264 the bulk sample consists in phenocrysts (49% felsic and corroded; 9% mafic), semi-opaque
265 scoriae including crystals (28%), opaque minerals (13%) and colorless to brownish transparent
266 vesiculated glass shards (2%); (2) basic feldspars represent the majority of the felsic group (Fig.
267 6); (3) The chemical composition of the glass shards is similar to those described for PU-II-P2-11
268 (Fig. 5f). The heavy mineralogy is dominated by orthopyroxenes (87%).
269

Correlation of the recent tephra layers (short cores)

Here, we propose a correlation model between the short (< 1m) sediment cores collected in Puyehue Lake, keeping in mind the possibility of mineralogical variations for a single tephra deposit, even on short distances (e.g., the May 1980 tephra of Mt St Helens, USA — Juvigné and Shipley, 1983). Due to the high purity of the heavy minerals studied in the tephra layers of PU-II-P2 and PU-I-P1 pilot cores (no contamination by the host sediment), the heavy mineral suite of tephras identified in short cores and in the upper meter of PU-II long core has been studied in details and used as a correlation tool. Correlations between cores PU-II-P2 and PU-I-P1 are also based on the geochemical data obtained on glass shards (similarity coefficients, Table 2). For correlation purposes, tephras have been numbered T1 to T5 according to their occurrence in PU-II-P2 pilot core and in the upper meter of PU-II long core (Fig. 2).

T1 and **T2** are easily recognized macroscopically (green color, fine grained material) and have been identified in all the cores collected in the western part of the lake (PU-SC1, PU-SC2, PU-II-P2 and PU-II long core, see Fig. 2). The detailed study of the geochemical composition of the glass shards of these tephras in PU-II-P2 has demonstrated that they can not be differentiated in terms of geochemistry (SC: 0.96). Some of the green layers occurring in the upper 25 centimeters of PU-SC7 should correspond to T1 and T2 tephras. Similarly, PU-I-P1-48 tephra probably corresponds to T1 or T2 (SC: 0.94 and 0.97, respectively). This correlation is supported by the bulk nature of the tephras: PU-I-P1-48 is a pumice lapilli containing a lot of vesiculated glass shards, and PU-II-P2-4 and PU-II-P2-8 are green fine-grained layers, typically originating from the in-situ weathering of fine-grained pumices (Bertrand et al., 2008). The difference between the grain-size of the tephra in the two cores is due to the difference in distance between the coring sites and PCCVC (Fig. 1). Pumices that reached PU-I site during the AD 1960

294 eruption of Cordon de Caulle were typically thicker and coarser than pumices deposited at PU-II
295 site (Wright and Mella, 1963).
296
297 **T3**: tephra layers PU-II-P2-11 and PU-I-P1-54 have five similar mineralogical and
298 geochemical characteristics that were not found in the other tephras occurring in the short cores
299 and in the upper five meters of the PU-II long core:
300 (1) The bulk fraction is dominated by phenocrystals;
301 (2) The heavy mineral fraction contains more than 80% of orthopyroxene;
302 (3) These tephras both contain dark brown amphibole (tchermakite);
303 (4) Free vesiculated glass shards are rare, and their geochemical composition ranges from
304 dacite to rhyolite (Fig. 5);
305 (5) Most of the feldspars are of basic composition (Fig. 6) and coated by lowly vesiculated
306 rhyodacitic glass.
307 These characteristics (in PU-II-P2 and PU-I-P1) are so unique that these tephras certainly
308 represent the same eruption. Moreover, the only statistically significant correlation of tephra
309 PU-II-P2-11 is with PU-I-P1-54 (SC: 0.94, Table 2). Based on the high proportion of
310 orthopyroxene in the heavy mineral suite and on the occurrence of brown amphibole, this
311 tephra was easily identified and correlated in PU-II long core (16 cm) and in four of the short
312 cores (PU-SC1/3/4/7). This tephra is missing in PU-SC2 short core (Fig. 2).
313
314 **T4**: In PU-II-P2 short core, the fourth tephra occurs at 42 cm. Its heavy mineral suite is
315 dominated by olivine (77%), which occurs in association with orthopyroxene (11%) and
316 clinopyroxene (8%). Based on the high percentage of olivine, this layer is correlated with tephras

317 in PU-SC2 short core and PU-II long core (Fig. 2). This correlation is confirmed by the high
318 magnetic susceptibility signal of this tephra layer in every core where it occurs (Bertrand et al.,
319 2005).
320
321 **T5**: A fifth tephra layer has been recognized in the upper meter of PU-II long core (PU-II-79).
322 Its heavy mineral suite is dominated by a two pyroxene association (orthopyroxene 45-62%;
323 clinopyroxene 33-47%), which allows us to differentiate it from other tephras and to propose a
324 correlation with tephras occurring at the base of five short cores (PU-SC1, 2, 3, 4, 7; Fig. 2).
325
326 *Age and origin of historical tephras*
327 Since regional historical eruptions are frequently characterized by the same geochemical and
328 mineralogical composition (Gerlach et al., 1988; González-Ferrán, 1994; Lara et al., 2004),
329 reconstructing the origin of each tephra layer remains a difficult challenge. However, the tephras
330 deposited in Puyehue Lake during the last millennium have been dated by different methods
331 (^{210}Pb, ^{137}Cs, varve-counting — Arnaud et al., 2005; Boës and Fagel, 2008), which allow us to
332 compare the succession of tephra layers in the sedimentary record to historical chronicles and to
333 attribute a probable origin to each tephra layer.
334
335 **T1**: In PU-II short core, the T1 tephra occurs in association with a 2.5 cm thick homogeneous
336 event deposit (Bertrand et al., 2005). This deposit has been dated at AD 1962 ± 2 by ^{210}Pb
337 (Arnaud et al., 2006) and at AD 1960 ± 0 by varve-counting (Boës and Fagel, 2008). The age of
338 this tephra layer demonstrates its association to the AD 1960 eruption of the PCCVC, which is
339 confirmed by the SC between this tephra and the lavas associated to the AD 1960 eruption (SC:

0.92, Table 2). This interpretation is also in good agreement with the rhyodacitic composition of its glass shards (Gerlach et al., 1988; Lara et al., 2004; Fig. 5g) and with the isopach map of Wright and Mella (1963). In Argentina, the AD 1960 Cordon de Caulle tephra has been identified in the sediments of lake Nahuel Huapi and in the collections of the Patagonia Museum at San Carlos de Bariloche. Both samples have a similar dacitic signature (Daga et al., 2006). However, because of the westerly winds prevailing during the AD 1960 eruption of the Cordon de Caulle (Wright and Mella, 1963), the AD 1960 tephra is much coarser in Argentina (Daga et al., 2006) than in the sediments of Puyehue Lake. Close to PCCVC, the AD 1960 tephra deposits consist in coarse lapilli pumice-fallout particles (Lara et al., 2006).

T2: The second tephra recorded at PU-II site (T2) has been dated by ^{210}Pb at AD 1922 ± 4 (Arnaud et al, 2006). This fine green layer has not been recognized in the thin sections used for varve-counting. According to the ^{210}Pb age and to the rhyodacitic composition of the glass shards of this tephra layer, it can be related to the AD 1921-22 eruption of Cordon de Caulle volcano (González-Ferrán, 1994). The SC between this tephra and the lavas emitted by Cordon de Caulle in AD 1921-22 (CCV unit of Gerlach et al., 1988) agrees with this interpretation (0.96). During this eruption that was characterized by a 6.2 km high tephra column (Lara et al., 2006), high quantities of pumices and ashes were emitted and transported by winds until Argentina (González-Ferrán, 1994). The T2 tephra has also been identified in the sediments of lake Nahuel Huapi, where it has a dacitic composition and is characterized by a high proportion of pumice clasts (Daga et al., 2006).

T3: The T3 tephra has been recognized in most of the sediment cores collected in Puyehue Lake (Fig. 2). According to the ^{210}Pb dating of PU-II short core, the age of T3 is AD 1902 ± 5

(Arnaud et al., 2006). The varve-counting age of T3 in PU-II pilot core is AD 1926 ± 3 and is inconsistent with its varve-counting age in PU-I pilot core (AD 1772 ± 18; Boës and Fagel, 2008). However, the mineralogical and geochemical composition of this tephra layer have demonstrated its very unique characteristics (see previous paragraph), giving to this correlation a very high reliability, which is supported by the high value of the similarity coefficient between PU-II-P2-11 and PU-I-P1-54 (0.94). The correlation is also strengthened by the magnetic susceptibility data (Bertrand et al., 2005) and by the occurrence of the T3 tephra at the end of the excess ^{210}Pb profiles in both PU-I and PU-II short gravity cores (Boës and Fagel, 2008). Although the AMS radiocarbon dates obtained on the bulk sediment samples bracketing the T3 tephra in cores PU-I-P1 and PU-II-P2 are biased by old carbon, they provide evidence that the two tephras were deposited concomitantly (similar age range for the two tephras, see Table 3).

The feldspars occurring in the T3 tephra and those emitted during the AD 1921-22 eruption of Cordon de Caulle show a very distinct geochemical composition (Fig. 6), demonstrating that the T3 tephra cannot be associated with the AD 1921-22 eruption of PCCVC. Moreover, the basic composition of the feldspars (Labradorite, Bytownite) occurring in T3 are incompatible with the chemical composition of their glass coating (rhyodacite) implying that the feldspars and their glass coating formed in distinct magma chambers. The feldspars probably crystallized in a first deep basic batholite, from which they ascended to reach a highly differentiated and shallow magma chamber where they acquired their rhyodacitic glass coating. In addition, the wide range of feldspar composition of these clean and unzoned crystals might also indicate an incorporation of xenocrystic material during the eruption. The only regional eruption that can explain such characteristics is the AD 1907 eruption of Rininahue Maar (Ducloux, 1908; Gerlach et al., 1988). This eruption was characterized by emissions of volcanic ashes reaching Valdivia (Chile) and Nahuel Huapi (Argentina) during 3 days (Ducloux, 1908; Gerlach et al., 1988). The only

388 analytical data available for the AD 1907 eruption of the Rininahue maar is the bulk geochemical
389 composition of the volcanic ashes collected on lake Nahuel Huapi directly after the eruption
390 (Ducloux, 1908). The tephra has a bulk andesitic composition, but no volcanic glasses were
391 analyzed separately. Although this tephra has reached Nahuel Huapi (Ducloux, 1908), it was not
392 observed in the BR sediment core taken in the northwestern part of the lake (Daga et al., 2006).
393 The T3 tephra is therefore dated at AD 1907, which is in agreement with its ^{210}Pb age but
394 inconsistent with the varve-counting age models. In PU-II short core, the varve-counting age of
395 the T3 tephra is 20 years too young. This difference is probably due to erosion and/or
396 destratification of several sediment layers deposited prior to AD 1960 by the strong AD 1960
397 seismo-tectonic event.
398
399 **T4**: The T4 tephra has only been found in the south-westernmost sediment cores and the
400 geochemical composition of its glass shards (basaltic andesite) is very different from the other
401 tephras (Fig. 5d). Although this tephra is too old to be dated by radionuclides, its varve-counting
402 age in PU-II pilot core provides evidence that it was deposited around AD 1590 ± 12 (Boës and
403 Fagel, 2008). If we take into account that varve-counting in PU-II-P2 overestimates the true ages
404 by ~20 years, this gives an age of AD 1570 ± 12 for the deposition of the T4 tephra. The only
405 eruption reported in historical documents and matching this date is the AD 1575 eruption of
406 Osorno volcano. This relation is supported by the basaltic to andesitic (51.67–54.41 % SiO_2)
407 nature of the effusive products generally emitted by the Osorno volcano (González-Ferrán, 1994),
408 which matches the composition of the T4 glass shards (Fig. 5d). Moreover, the T4 tephra only
409 occurs in the southeastern part of the lake, which is in agreement with a southern origin for the
410 tephra particles (see location of Osorno volcano in Fig. 1).

411

412 **T5**: The T5 tephra is characterized by a 2 pyroxene association. In PU-II long core, it is dated
413 at AD 980 ± 15 by extrapolation of the radiocarbon age model. According to Lopez-Escobar et
414 al. (1995), the two-pyroxene association ± Fe-olivine is characteristic for dacites and rhyolites of
415 the central province of the SVZ. However, most of the volcanic products of the PCCVC contain
416 an association of ortho- and clino-pyroxenes. The origin of this tephra layer is still not defined.
417 No historical chronicles are available for this period.

418

419 *Comparison with previous models*

420 In PU-I-P1, the volcanoclastic layer associated to PU-I-P1-48 tephra occurs 6 to 10 cm above
421 the T3 tephra, which we associate to the AD 1907 eruption of Rininahue volcano (Fig. 2). Based
422 on its stratigraphic position and to the geochemical composition of its glass shards (rhyodacite), it
423 can be correlated to one of the two recent eruptions of the PCCVC (AD 1921-22 or AD 1960).
424 However, these eruptions are mineralogically and geochemically similar (SC > 0.92, see Table 2)
425 and we have therefore no argument to determine if this deposit corresponds to T1 or to T2, which
426 can not be differentiated from each other based on mineralogical and geochemical data (Daga et
427 al., 2006; this work). This is in contrast with Chapron et al. (2007) who use the glass shard
428 geochemical composition of PU-I-P1-48 to affirm that these particles originate from the
429 remobilization of Cordon de Caulle AD 1960 fallout particles previously deposited in the lake
430 catchment.

431

432 According to the varve-couting age of T3 in PU-II pilot core (AD 1926 ± 3), Bertrand et al.
433 (2005) and Böes and Fagel (2008) proposed to link this tephra to the AD 1921-22 eruption of
434 Cordon de Caulle. However, the bulk mineralogical composition of this tephra (very low content

435 of glass shards) and the geochemical composition of its plagioclase compared to the plagioclase
436 associated to the AD 1921-22 eruption of Cordon de Caulle (Fig. 6) allow us to refute this
437 hypothesis. This tephra layer is now associated to the AD 1907 eruption of Rininahue volcano,
438 which is in better agreement with the radionuclides data.
439
440 *Prehistorical tephras*
441
442 *Characterization of the tephra layers occurring in PU-II long core (Figs. 7 and 8)*
443 Here, we present the mineralogical and geochemical composition of the 15 thickest tephras
444 identified in PU-II long core (i.e., those who have a high probability to be widespread in the
445 region and a low probability to be contaminated by particles from the host sediment). This
446 provides a continuous 18,000 years tephra database, which will be useful to correlate future
447 paleoenvironmental and paleoclimatological records and to refine the age models of regional
448 sedimentary archives.
449
450 The main characteristics of the 15 prehistorical tephras selected for analysis are presented in
451 Figure 7 (mineralogy), Figure 8 (geochemistry) and Supplementary Tables 2 and 3. The data
452 demonstrate that several tephras have similar mineralogical compositions, which seem to be
453 characteristic for the region. Ten tephras are characterized by a bulk composition dominated by
454 abundant scoriae (referred to as TC1 for typical composition 1 in Supplementary Table 2) and
455 eleven have a heavy mineral suite essentially composed of ortho-, and clinopyroxene (TC2 in
456 Supplementary Table 2). Several tephras (PU-II-419, 929, 933) contain two geochemically-
457 distinct populations of glass shards that could indicate that the eruption has been triggered by
458 magma mixing.

459

460 *Age and origin of tephras analyzed in PU-II long core*

461 In spite of the prevailing westerly winds that transported most of the eruptive products eastward
462 (Besoain, 1985), numerous tephras have reached Puyehue Lake during the last 18,000 years. The
463 age of the tephras, which has been calculated from the AMS radiocarbon age model presented in
464 Bertrand et al. (2008), demonstrates they have been regularly deposited at PU-II site throughout
465 the last 18,000 years, with no significant temporal trend (Fig. 3). This indicates that the Southern
466 Volcanic Zone has been constantly active throughout the last 18,000 years. In the literature, it has
467 been proposed that glacial unloading may have caused an increase in volcanic activity, especially
468 during the last deglaciation (Rampino et al., 1979; Hall, 1982). Although this topic is still debated
469 (e.g., Zielinski et al., 1996, Castellano et al., 2004), we show here that there is no relation
470 between the frequency of volcanic eruptions and abrupt climate changes in the Puyehue area (Fig.
471 3). Even if the deglaciation in the region happened quickly (McCulloch et al., 2000), it seems that
472 the rapid glacial unloading did not affect the volcanic activity of the Central province of the
473 Southern Volcanic Zone of Chile, in agreement with the results of Gerlach et al. (1988) who
474 show that volcanism in the Puyehue-Cordon de Caulle area began in an intraglacial period (less
475 than 200,000 years ago).

476

477 Most of the tephras deposited in Puyehue Lake are supposed to originate from nearby
478 volcanoes (see Fig. 1), and more particularly from PCCVC, which is very close to the lake and
479 which has been active for the last 200,000 years (Gerlach et al., 1998). Trying to reconstructing
480 the source of every tephra is unreasonable but the mineralogical and geochemical data can help to
481 better constrain the type of eruption and/or the distance from the eruptive center. Our data
482 demonstrate that most of the analyzed tephras display a heavy mineral suite dominated by the

two-pyroxene association (ortho- and clinopyroxene). As stated by Lopez-Escobar et al., (1995), this association seems to be characteristic for the central province of the SVZ and is in agreement with a local origin of the particles. The tephras originating from highly differentiated magmas and characterized by vesiculated glass shards (e.g., PU-II-79, 255, 633, 901, 929) might originate from more distant volcanoes. In addition, the presence of olivine in several tephras (PU-II-377, 419, 490, 1003 and 1005) might indicate an origin from the nearby Antillanca volcanic complex.

Because some of the analyzed tephras are characterized by very unique mineralogical and geochemical compositions, these layers are very promising in terms of stratigraphic correlations. For example, tephra PU-II-633 is very rich in amphibole and therefore easily discernible from other layers. This confers to this tephra a high potential for correlation between sites. In addition, tephras PU-II-79, 633 and 901 are abnormally rich in colorless glass shards (highly differentiated magma, pumices). Because of the high dispersion of such volcanic products, these tephras can be very useful to correlate sedimentary records over long distances. Tephras dominated by dark grey scoria are probably less useful for long distance correlations.

In their study of the volcanic lavas emitted by the PCCVC over 200,000 years, Gerlach et al. (1988) demonstrated an evolution from basaltic to more silicic lavas through time, with the postglacial lavas being mainly silicic (rhyodacite and rhyolite). Our results demonstrate that during the last 18,000 years, regional volcanoes have emitted lavas with a composition ranging from basaltic andesite to rhyolite, without any trend to more silicic lavas through time. The tephras deposited in Puyehue Lake between 13,000 and 15,000 cal. yr. BP (PU-II-901, 929, 933) were already silicic in nature (rhyolite to andesite). Therefore, we argue that silicic products, similar to those emitted by the Cordon de Caulle in AD 1921-22 and AD 1960, have been

emitted throughout the post-glacial period and that the trend observed by Gerlach et al. (1998) is a long term (200,000 years) trend, which does not affect the late Pleistocene and Holocene tephras.

Conclusion

This study provides the first tephrostratigraphic database for south-central Chile (36-42°S) and demonstrates that the central province of the SVZ has been volcanologically active throughout the last 18,000 years, with no increase in volcanic activity during glacial unloading. The geochemical data demonstrate that regional volcanoes have emitted particles with a composition ranging from basaltic andesite to rhyolite without any evidence of magma evolution through time. The heavy mineralogy of tephras emitted during the last 18,000 years is typically characterized by a two-pyroxene association. Several tephras are very promising in terms of long distance stratigraphic correlations, either because they present very unique geochemical and/or mineralogical characteristics (e.g., PU-II-633) or because of their high content in vesiculated glass shards, characteristic for highly dispersed tephras (e.g., PU-II-79, 633, 901). For the last millennium, we show that the sediments of Puyehue Lake have recorded five major eruptions characterized by distinct volcanic products: T1 and T2 are related to the AD 1960 and AD 1921-22 eruptions of PCCVC and can not be differentiated from each other based on their mineralogical and geochemical characteristics; T3 is a crystal-rich tephra related to the AD 1907 eruption of Rininahue maar; T4 is an olivine-rich tephra tentatively associated to the AD 1575 eruption of Osorno volcano; T5 has a heavy mineralogical suite dominated by both clino- and ortho-pyroxene in equivalent proportions and can be used as a tephrochronological marker for the second half of the first millennium AD. Finally, this work demonstrates that a pluridisciplinary

approach is required for accurately understanding lake sedimentary records, especially is such a highly active geodynamic setting.

Acknowledgments

The ENSO-Chile project is supported by the Belgian Federal Office for Scientific, Technical and Cultural Affairs (OSTC). Thanks are due to Elisabeth Tallier and Virginie Renson for core sampling and laboratory assistance. Jacques Wautier (CAMST, Louvain-la-Neuve) is acknowledged for the microprobe analyses. Marc De Batist and the ENSO-Chile project members are thanked for fruitful scientific discussions. Finally, we wish to thank Mike Kaplan and an anonymous reviewer for their constructive comments and suggestions.

References

Arnaud, F., Magand, O., Chapron, E., Bertrand, S., Boës, X., Charlet, F., Mélières, M.A., 2006. Radionuclides dating (^{210}Pb, ^{137}Cs, ^{241}Am) of recent lake sediments in a highly active geodynamic setting (Lakes Puyehue and Icalma — Chilean Lake District). Science of the Total Environment 366, 837–850.

Besoain, E. 1985. Mineralogía de los suelos volcánicos del centro-sur de Chile. Suelos volcánicos de Chile. In: Tosso, J. (Ed.), Suelos volcanicos de Chile. Instituto de Investigaciones Agropecuarias (INIA), Santiago, pp. 108–152.

554 Bertrand S., Fagel N., 2008. Nature, origin, transport and deposition of andosol parent material in
555 south-central Chile (36-42°S). Catena 73, 10–22.
556
557 Bertrand, S., Boës, X., Castiaux, X., Charlet, F., Urrutia, R., Espinoza, C., Lepoint, G., Charlier,
558 B., Fagel, N. 2005. Temporal evolution of sediment supply in Lago Puyehue (Southern Chile)
559 during the last 600 years and its climatic significance. Quaternary Research 64, 163–175.
560
561 Bertrand, S., Charlet, F., Charlier, B., Renson, V., Fagel, N., 2008. Climate variability of
562 Southern Chile since the Last Glacial Maximum: a continuous sedimentological record from
563 Lago Puyehue (40°S). Journal of Paleolimnology 39, 179–195.
564
565 Blott, S. J., Pye, K., 2001. Gradistat: a grain size distribution and statistics package for the
566 analysis of unconsolidated sediments: Earth Surface Processes and Landforms 26, 1237–1248.
567
568 Boës, X., Fagel, N., 2008. Relationships between southern Chilean varved lake sediments,
569 precipitation and ENSO for the last 600 years. Journal of Paleolimnology 39, 237–252.
570
571 Borchardt, G.A., Aruscavage, P.J., Mallard Jr., H.P., 1972. Correlation of the Bishop Ash, a
572 Pleistocene marker bed, using instrumental neutron activation analysis. Journal of Sedimentary
573 Petrology 42, 301–306.
574
575 Boygle, J., 1999. Variability of tephra in lake and catchment sediments, Svínavatn, Iceland.
576 Global and Planetary Change 21, 129–149.
577

578 Calderoni, G., Turi, B., 1998. Major constraints on the use of radiocarbon dating for
579 tephrochronology. Quaternary International 47-48, 153–159.
580
581 Castellano, E., Becagli, S., Jouzel, J., Migliori, A., Severi, M., Steffensen, J.P., Traversi, R.,
582 Udisti, R., 2004. Volcanic eruption frequency over the last 45 ky as recorded in Epica-Dome C
583 ice core (East Antarctica) and its relationship with climatic changes, Global and Planetary 42,
584 195−205.
585
586 Chapron, E., Juvigné, E., Mulsow, S., Ariztegui, D., Magand, O., Bertrand, S., Pino, M.,
587 Chapron, O., 2007. Recent clastic sedimentation in Lake Puyehue (Chilean Lake District,
588 40.5°S). Sedimentary Geology 201, 365–385.
589
590 Charlet, F., De Batist, M., Chapron, E., Bertrand, S., Pino, M., Urrutia, R., 2008. Seismic-
591 stratigraphy of Lago Puyehue (Chilean Lake District): new views on its deglacial and Holocene
592 evolution. Journal of Paleolimnology 39, 163–177.
593
594 Daga, R., Guevara, S.R., Sánchez, M.L., Arribére, M., 2006. Geochemical characterization of
595 volcanic ashes from recent events in Northern Patagonia Andean Range by INAA. Journal of
596 Radioanalytical and Nuclear Chemistry 270 (3), 677–694.
597
598 De Batist, M., Fagel, N., Loutre, M.-F., Chapron, E., 2008. A 17,900-year multi-proxy lacustrine
599 record of Lago Puyehue (Chilean Lake District): introduction. Journal of Paleolimnology 39,
600 151–161.
601

602 de Fontaine, C.S., Kaufman, D.S., Anderson, R.S., Werner, A., Waythomas, C.F., Brown, T.A.,
603 2007. Late Quaternary distal tephra-fall deposits in lacustrine sediments, Kenai Peninsula,
604 Alaska. Quaternary Research 68, 64−78.
605
606 Ducloux, E.H., 1908. Ceniza del volcán Rininahue. Revista del museo de La Plata 15, 49–53.
607
608 Froggatt, P.C., 1992. Standardisation of the chemical analysis of tephra deposits. Report on the
609 ICCT working group. Quaternary International 13-14, 93–96.
610
611 Gerlach, D.C., Frey, F.A., Moreno, H., Lopez-Escobar, L., 1988. Recent volcanism in the
612 Puyehue-Cordon Caulle Region, Southern Andes, Chile (40.5°S): Petrogenesis of evolved lavas.
613 Journal of Petrology 29, 333–382.
614
615 González-Ferrán, O., 1994. Volcanes de Chile. Instituto Geografico militar, Santiago, Chile, 635
616 pp.
617
618 Haberle, S.G., Lumley, S.H., 1998. Age and origin of tephras recorded in postglacial lake
619 sediments to the west of the southern Andes, 44°S to 47°S. Journal of Volcanology and
620 Geothermal Research 84, 239–256.
621
622 Hajdas, I., 1993. Extension of the radiocarbon calibration curve by AMS dating of laminated
623 sediments of lake Soppensee and lake Holzmaar. Unpublished PhD thesis, ETH Zurich,
624 Switzerland.
625

626 Hall, K., 1982. Rapid deglaciation as an initiator of volcanic activity: An hypothesis. Earth
627 Surface Processes and Landforms 7, 45–51.
628
629 Hallet, D. J., Mathewes, R.W., Foit, F. F., Jr., 2001. Mid-Holocene Glacier Peak and Mount St.
630 HelensWe tephra layers detected in lake sediments from Southern British Columbia using high
631 resolution techniques. Quaternary Research 55**,** 284–292.
632
633 Hickey, R.L., Gerlach, D.C., Frey, F.A., 1984. Geochemical variations in volcanic rocks from
634 central south Chile (33°S-42°S): implications for their petrogenesis. In: Harmon R.S. and
635 Barreiro D.A. (eds), Andean Magmatism: Chemical and isotopic constraints. Shiva Publications
636 Limited, Cheshire, United Kingdom, pp. 72–95.
637
638 Hodder, A.P.W., De Lande P. J., Lowe, D.J., 1991. Dissolution and depletion of ferromagnesian
639 minerals from Holocene tephra layers in an acid bog, New Zealand, and implications for tephra
640 correlation. Journal of Quaternary Science 6, 195–208.
641
642 Hodgson, D.A., Dyson, C.L., Jones, V.J., Smellie, J.L., 1998. Tephra analysis of sediments from
643 Midge Lake (South Shetland Islands) and Sombre Lake (South Orkney Islands), Antarctica.
644 Antarctic Science 10, 13–20.
645
646 Hunt, J. B., and Hill, P. G. (1993). Tephra geochemistry: A discussion of some persistent
647 analytical problems. The Holocene 3**,** 271–278.
648

649 Juvigné, E., 1983. Les variations minéralogiques dans les retombées de 1982 du volcan El
650 Chichon (Chiapas, Mexique) et leur intérêt pour la téphrostratigraphie. Annales de la Société
651 géologique de Belgique 106, 311–325.
652
653 Juvigné, E., 1993. Contribution à la téphrostratigraphie du Quaternaire et son application à la
654 géomorphologie. Mem. Expl. Cartes Geol. Min. Belgique, Bruxelles, 36, 66 pp.
655
656 Juvigné, E., Shipley, S., 1983. Distribution of heavy minerals in the downwind lobe of the May
657 18, 1980 eruption of the Mount St Helens (Washington, USA). Eiszeitalter und Gegenwart 33, 1–
658 7.
659
660 Kilian, R., Hohner, M., Biester, H., Wallrabe-Adams, H.J., Stern, C.J., 2003. Holocene peat and
661 lake sediment tephra record from the southernmost Chilean Andes (53-55°S). Revista Geologica
662 de Chile 30, 23–37.
663
664 Lara, L.E., Naranjo, J.A., Moreno, H., 2004. Rhyodacitic fissure eruption in Southern Andes
665 (Cordon Caulle; 40.5°S) after the 1960 (MW: 9.5) Chilean earthquake: a structural
666 interpretation. Journal of Volcanology and Geothermal Research 138, 127–138.
667
668 Lara, L.E., Moreno, H., Naranjo, J.A., Matthews, S., Pérez de Arce, C., 2006. Magmatic
669 evolution of the Puyehue-Cordon de Caulle Volcanic Complex (40°S), Southern Andean
670 Volcanic Zone: From shield to unusual rhyolitic fissure volcanism. Journal of Volcanology and
671 Geothermal Research 157, 343–366.
672

673 Laugenie, C., 1982. La région des lacs, Chili méridional. Unpublished PhD Thesis, Université de
674 Bordeaux III, France.
675
676 Le Bas, N.J., Le Maitre, R.W., Streckeinsen, A., Zanetin, B. 1986. A chemical classification of
677 volcanic rocks based on Total Alkali-Silica diagram. Journal of Petrology 27, 745–750.
678
679 Litt, T., Schmincke, H.-U., Kromer, B., 2003. Environmental response to climatic and volcanic
680 events in central Europe during the Weischselian Lateglacial. Quaternary Science Reviews 22,
681 7–32.
682
683 Lopez-Escobar, L., Moreno, H., 1981. Erupción de 1979 del volcan Mirador, Andes del Sur,
684 40°21' S: características geoquímicas de las lavas y xenolitos graníticos. Revista geológica de
685 Chile 13-14, 17–33.
686
687 Lopez-Escobar, L., 1984. Petrology and geochemistry of volcanic rocks of the southern Andes.
688 In: Harmon R.S. and Barreiro B.A. (eds) Andean magmatism - Chemical and isotopic constraints.
689 Shiva Publications Limited, Cheshire, United Kingdom, pp. 47–71.
690
691 Lopez-Escobar, L., Frey, F. A., Vergara, M., 1977. Andesites and high-alumina basalts from the
692 central–south Chile High Andes: geochemical evidence bearing on their petrogenesis.
693 Contributions to Mineralogy and Petrology 63, 199–228
694

695 Lopez-Escobar, L., Cembrano, J., Moreno, H., 1995. Geochemistry and tectonics of the Chilean
696 Southern Andes basaltic Quaternary volcanism (37-46°S). Revista Geologica de Chile 22, 219–
697 234.
698
699 McCulloch, R.D., Bentley M.J., Purves, R.S., Hulton, N.R.J., Sudgen, D.E., Clapperton, C.M.,
700 2000. Climatic inferences from glacial and palaeoecological evidence at the last glacial
701 termination, southern South America. Journal of Quaternary Science 15, 409–417
702
703 Moreno, H., 1977. Geologia del area volcanica Puyehue Carran en Los Andes del Sur de Chile.
704 PhD thesis, Univ. de Chile, Santiago, 170 pp.
705
706 Naranjo, J., Stern, C. 2004. Holocene tephrochronology of the southernmost part (42°30'–45°S)
707 of the Andean Southern Volcanic Zone. Revista Geologica de Chile 31, 225–240.
708
709 Newnham, R. M., Lowe, D. J., 1999. Testing the synchroneity of pollen signals using
710 tephrostratigraphy. Global and Planetary Change 21, 113–128.
711
712 Newton, A.J., Metcalfe, S.E., 1999. Tephrochronology of the Toluca Basin, central Mexico.
713 Quaternary Science Reviews 18, 1039–1059.
714
715 Ortega-Guerrero, B., Newton, A.J., 1998. Geochemical characterisation of Late Pleistocene and
716 Holocene tephra layers from the basin of Mexico, Central Mexico. Quaternary research 50, 90–
717 106.
718

719 Rampino, M.R., Self, S., Fairbridge, R.W., 1979. Can rapid climatic change cause volcanic
720 eruptions? Science 206, 826–829.
721
722 Schmidt, R., van den Bogaard, C., Merkt, J., Müller J., 2002. A new Lateglacial
723 chronostratigraphic tephra marker for the south-eastern Alps: The Neapolitan Yellow Tuff (NYT)
724 in Längsee (Austria) in the context of a regional biostratigraphy and palaeoclimate. Quaternary
725 International 88, 45–56.
726
727 Shane, P., Lian, O.B., Augustinus, P., Chisari, R., Heijnis, H., 2002. Tephrostratigraphy and
728 geochronology of a ca. 120 ka terrestrial record at Lake Poukawa, North Island, New Zealand.
729 Global and Planetary Change 33, 221–242.
730
731 Sterken, M., 2003. Changes in diatom preservation, community structure and production after
732 tephra deposition in Lago Puyehue (Chile): A paleolimnological approach. Unpublished M.Sc.
733 thesis, UGent, Belgium.
734
735 Stern, C. R., 1989. Pliocene to present migration of the volcanic front, Andean Southern Volcanic
736 Zone. Revista Geologica de Chile 16, 145–162.
737
738 Stuiver, M., Reimer, P.J., Bard, E., Beck, J.W., Burr, G.S., Hughen, K.A., Kromer, B.,
739 McCormac, G., van der Plicht J., Spurk M., 1998. Intcal98 radiocarbon age calibration, 24,000-0
740 cal BP. Radiocarbon 40, 1041–1083.
741

742 Telford, R.J., Barker, P., Metcalfe, S., Newton, A., 2004. Lacustrine responses to tephra
743 deposition: examples from Mexico. Quaternary Science Reviews 23, 2337–2353.
744
745 Thornton, C., Tuttle, O., 1960. Chemistry of igneous rocks. Part I, Differentiation Index.
746 American Journal of Sciences 258, 664–684.
747
748 Wright, C., Mella, A., 1963. Modifications to the soil pattern of south-central Chile resulting
749 from seismic and associated phenomena during the period May to August 1960. Bulletin of the
750 Seismological Society of America 53, 1367–1402.
751
752 Wulf, S., Kraml, M., Brauer, A., Keller, J., Negendank, J.F.W., 2004. Tephrochronology of the
753 100 ka lacustrine sediment record of Lago Grande di Monticchio (southern Italy). Quaternary
754 International 122, 7–30.
755
756 Zielinski, G.A., Mayewski, P.A., Meeker, L.D., Whitlow, S.I., Twickler, M.S., 1996. A 110,000-
757 yr record of explosive volcanism from the GISP2 (Greenland) ice core. Quaternary Research 45,
758 109–118.

759 **Table captions**

760

761 **Table 1** – Electron microprobe analytical conditions and standards used for calibration (natural
762 and synthetic minerals with published composition data). Acceleration voltage 15 kV, beam
763 current 6 nA, beam diameter 25 μm.

764

765 **Table 2 –** Similarity coefficient (SC) calculations (after Borchardt et al, 1972) comparing major
766 element analysis of tephras from PU-II-P2 and PU-I-P1 short cores. The coefficients are
767 calculated using the geochemical data (SiO_2, Al_2O_3, FeO, CaO, Na_2O and K_2O) presented in
768 Supplementary Table 3. We used unit weighting (1.0) of the oxide concentrations of Si, Al, and
769 Fe, and quarter weighting (0.25) of the oxide concentrations of Ca, Na, K. These were given
770 lower weighting because of their low concentrations and, consequently, high relative error of
771 measurement (Hallett et al., 2001). Values ≥ 0.92 (highlighted in bold) are generally taken as
772 indicative of correlation between tephra samples (Froggatt, 1992).

773

774 **Table 3** – AMS radiocarbon ages obtained on bulk sediment samples bracketing the T3 tephra in
775 PU-I-P1 and PU-II-P2 short cores. Radiocarbon dates were calibrated at the 95.4% confidence
776 interval by OxCal 3.5, using atmospheric data of Stuiver et al. (1998). The absolute radiocarbon
777 ages are ~ 600 years older than the real age of the T3 tephra (AD 1907). This age difference can
778 be explained by (1) incorporation of juvenile carbon emitted by the highly active regional
779 volcanoes (Hajdas, 1993; Calderoni and Turi, 1998) and (2) incorporation of organic matter
780 previously deposited in the lake watershed and containing old radiocarbon.

781

782 **Figure captions**

783

784 **Figure 1** – Map of Puyehue Lake and nearby volcanoes (modified from González-Ferrán, 1994).

785

786 **Figure 2** – Location and lithology of the short cores collected in the eastern part of Puyehue
787 Lake. The upper part of PU-II long core is also represented. Based on the nature of the heavy
788 mineral fraction, correlations between cores are proposed. Tephras T1 and T2 do not contain
789 heavy minerals and have a similar geochemical composition. They are therefore correlated
790 according to macroscopical descriptions only. Tephras have been attributed the following ages:
791 T1: AD 1960; T2: AD 1921-22; T3: AD 1907; T4: AD 1575; T5: unknown. See text for details.

792

793 **Figure 3** – Lithological column and age-model of PU-II long core (from Bertrand et al., 2008)
794 indicating the occurrence and the thickness of tephra layers. The age model is based on 9
795 calibrated radiocarbon dates (Bertrand et al., 2008) and 2 historically documented tephra layers
796 (this work). Error bars represent the 2 σ error range. Stars indicate tephra layers selected for
797 mineralogical and geochemical analysis (i.e., thicker than 6 mm). The upper part of the figure
798 represents the tephra thickness versus time and shows that the volcanic eruptions were well
799 distributed throughout the last 18,000 years, with no significant temporal trend.

800

801 **Figure 4** – Bulk grain-size distribution of 3 typical tephra samples occurring in PU-II long core.
802 All the samples contain a mixture of tephra particles and host sediment. Tephra grains were
803 separated from the host sediment by sieving the samples at 75 and 420 µm (see text). A) PU-II-
804 500: sample dominated by coarse tephra particles, where the host sediment only represents 10 %
805 of the total sample and is completely discarded after sieving at 75 µm; B) PU-II-744: sample

806 composed of a mixture of coarse tephra particles and host sediment. Particles coarser than 75 µm
807 may contain host sediment; C) PU-II-179: fine tephra layer. In this case the >75 µm fraction does
808 not contain all the tephra particles.
809
810 **Figure 5** – TAS classification (Le Bas et al., 1986) of the geochemical data obtained by
811 microprobe on the glass shards of historical tephras collected in the short cores PU-I-P1 and PU-
812 II-P2. For comparison, the geochemical composition of magma emitted during the eruption of the
813 Cordon de Caulle in AD 1921-22 and AD 1960 are represented (data from Gerlach et al., 1988).
814 Data are presented in Supplementary Table 3. Note that the glass shards from tephras PU-II-P2-
815 11 and PU-II-P1-54 (graphs C and F) contain a wide range of composition that is probably due to
816 the very low glass shard content of these samples (3 and 2%, respectively), increasing the risk of
817 contamination by glass shards from the host sediment.
818
819 **Figure 6** – Plagioclase composition of the T3 tephra collected in cores PU-I-P1 (53.5–54 cm) and
820 PU-II-P2 (10.8–11.2 cm). For comparison, the composition of plagioclase from lavas associated
821 to the 1921-22 eruption of Cordon de Caulle is represented (data from Gerlach et al., 1988). The
822 results demonstrate that the T3 tephra is not related to the 1921-22 eruption of Cordon de Caulle
823 and that the basic composition of the feldspars (labradorite, bytownite) is incompatible with the
824 chemical composition of their glass coating (rhyodacite), implying at least two distinct sources of
825 material.
826
827 **Figure 7** – Bulk and heavy mineralogy of the 15 thickest tephra layers collected in PU-II long
828 core. In addition, the three youngest tephras (PU-II-16, 59 and 79) are also represented. See
829 Supplementary Table 2 for more details.

Figure 8 – Geochemical results obtained by microprobe on glass shards from PU-II long core tephras. Tephras containing less than 15% of glass shards (see Supplementary Table 2) have not been analyzed for geochemistry. Magma composition is indicated in the TAS classification (Le Bas et al., 1986). A) Mean values in the general classification; B) Close-up for each sample; C) mean values in the K_2O-Na_2O diagram. Data are presented in Supplementary Table 3.

Online supplementary material

Supplementary Table 1 – Main characteristics of the tephra layers identified in the pilot and short cores collected in Puyehue Lake (see Fig. 2 for location). Heavy minerals representing less than 10 % of the total heavy fraction are not listed, except for brown amphibole which is an indicative mineral. Heavy minerals are abbreviated as follows: opx: orthopyroxene; cpx: clinopyroxene; oli: olivine; bb amp: brown amphibole. An age has been attributed to each tephra layer by comparing the results of different dating methods (^{210}Pb, ^{137}Cs, varve-counting) to historical chronicles: T1: AD 1960; T2: AD 1921-22; T3: AD 1907; T4: AD 1575; T5: unknown. See text for details.

Supplementary Table 2 – Main characteristics of the tephra layers analyzed in PU-II long core. Minerals representing less than 5 % of the total fraction are not indicated. The following abbreviations are used: (1) bulk mineralogy (op.: opaque; tr.: translucent; ves.: vesiculated; g.s. glass shards); (2) heavy mineralogy (opx: orthopyroxene; cpx: clinopyroxene; oli: olivine; gg amp: green amphibole; bg amp: green to brownish green amphibole; bb amph: brown amphibole). Normative corundum (CIPW norm) is an indicator of *in situ* glass chemical alteration. The differentiation index (Thornton and Tuttle 1960) is an indicator of oversaturation in Al. TC1/2 refers to "typical composition 1 (bulk composition dominated by abundant dark grey scoriae) and/or 2 (heavy mineral suite essentially composed of ortho-, and clinopyroxenes), respectively. Ages are derived from an AMS radiocarbon age model detailed in Bertrand et al. (2008) and presented in Figure 1. The real error bar on the radiocarbon dates is probably larger than indicated, but the error induced by incorporation of old radiocarbon (approx. 600 yrs for the recent deposits, see Table 3) is hardly quantifiable.

860

861 **Supplementary Table 3** – Puyehue tephra glass geochemistry (total dataset normalized to 100
862 wt %). Mn and Cr were all very low (below the limit of quantification) and are not included in
863 this table. [a] total Fe as FeO ; [b] from Gerlach et al (1988), normalized to 100 wt %. CC-1960 and
864 CC-1921-22 are bulk geochemical values obtained on lavas emitted during the AD 1960 and AD
865 1921-22 eruptions of the PCCVC, respectively. See Figures 5 and 8 for graphical representation
866 of the data.

867

Table 1

Element	Counting time (seconds)		Standard
	Peak	Background	
Na	16	8	Oligoclase
Mg	16	8	Olivine
Al	16	8	Synthetic saphir
Si	16	8	Wollastonite
Fe	10	5	Hematite
Ca	10	5	Wollastonite
Ti	10	5	Rutile
K	10	5	Leucite
Cr	10	5	Chromite
Mn	10	5	Rhodonite

Bertrand et al – Table 1

Table 2

	PU-II-P2-4	PU-II-P2-8	PU-II-P2-11	PU-II-P2-42	PU-I-P1-48	PU-I-P1-54	PU-II-79	CC1960	CC1921-22
PU-II-P2-4	-								
PU-II-P2-8	**0.96**	-							
PU-II-P2-11	0.90	0.90	-						
PU-II-P2-42	0.66	0.65	0.62	-					
PU-I-P1-48	**0.94**	**0.97**	0.87	0.66	-				
PU-I-P1-54	0.86	0.87	**0.94**	0.63	0.86	-			
PU-II-79	0.91	**0.95**	0.87	0.65	**0.97**	0.87	-		
CC-1960	**0.92**	**0.96**	0.89	0.64	**0.95**	0.87	**0.95**	-	
CC-1921-22	**0.96**	**0.96**	0.89	0.65	**0.95**	0.86	**0.92**	**0.96**	-

Bertrand et al – Table 2

Table 3

	Depth (cm)	^{14}C age ±1 σ	Calibrated age	Laboratory n°
PU-I-P1	54.0–54.5	640 ± 30	AD 1290–1400	Poz-16384
	55.0–55.5	530 ± 40	AD 1300–1450	Beta-213316
PU-II-P2	10.2–10.7	1160 ± 30	AD 770–980	Poz-16435
	11.2–11.7	630 ± 40	AD 1290–1410	Poz-16436

Bertrand et al – Table 3

Supplementary Table 1

Tephra label	Depth (cm)	Thickness (cm)	Color	Heavy mineralogy	Interpretation
PU-II-P2-4	4.0–4.5	0.5	Light green	--	T1
PU-II-P2-8	8.0–8.5	0.5	Light green	--	T2
PU-II-P2-11	10.8–11.2	0.4	Black	Opx (83%), cpx (13%), bb amph (2%)	T3
PU-II-P2-42	41.5–42.0	0.5	Black + red	Oli (77%), opx (11%)	T4
PU-I-P1-48	47.5–48.0	0.5 (+3.5)	Light gray	--	T1–T2
PU-I-P1-54	53.5–54.0	0.5	Black	Opx (87%), cpx (11%), bb amp (1.5%)	T3
PU-II-16	15.7–16.0	0.3	Black	Opx (76%), cpx (17%), bb amp (6%)	T3
PU-II-59	58.5–59.0	0.5	Black + red	Opx (38%), cpx (29%), oli (25%)	T4
PU-II-79	78.8–79.3	0.5	Black	Opx (62%), cpx (35%)	T5
PU-SC1-13	13.4–13.6	0.2	Black	Opx (76%), cpx (18%), bb amp (5%)	T3
PU-SC1-50	50.4–50.6	0.2	Black	Opx (48%), cpx (47%)	T5
PU-SC2-58	57.8–58.2	0.4	Black	Opx (33%), cpx (43%), oli (19%)	T4
PU-SC2-61	60.4–60.6	0.2	Black	Opx (52%), cpx (36%)	T5
PU-SC3-18	16.0–19.0	3.0	Black	Opx (70%), cpx (23%), bb amp (4%)	?
PU-SC3-35	35.5–35.8	0.3	Black	Opx (78%), cpx (13%), bb amp (9%)	T3
PU-SC3-52	51.5–52.0	0.5	Black	Opx (50%), cpx (41%), bb amp (2%)	T5
PU-SC4-18	18.5–19.2	0.7	Black	Opx (82%), cpx (14%), bb amp (4.3%)	T3
PU-SC4-82	82.0–82.2	0.2	Black	Cpx (49%), opx (44%), bb amp (1%)	T5
PU-SC7-51	50.0–50.5	0.5	Dark gray	Opx (80%), cpx (15%), bb amp (3%)	T3
PU-SC7-71	70.9–71.1	0.2	Black	Opx (45%), cpx (33%), bb amp (2.2%)	T5

Supplementary Table 2

Tephra label	Depth (cm)	Thickness (cm)	Grain-size mode (µm)	3 coarsest grains (mm)	Color	Bulk mineralogy	Heavy mineralogy	Magma comp.	Corundum %	Differen-ciation index	Comments and typical characteristics	Age (cal. yr. BP ± 2 σ)
PU-II-16	15.7–16.0	0.3	250		Black	Op. (12%) and tr. (27%) scoria; felsic phenocrystals (52%)	Opx (76%), cpx (17%), bb amp (6%)	--	--	--	See comments for T3 (short cores)	1908 AD
PU-II-59	58.5–59.0	0.5	215		Black + red	Op. (26%) and tr. (27%) scoria; brown g.s. (30%)	Opx (38%), cpx (29%), oli (25%)	--	--	--	See comments for T4 (short cores)	1570 AD
PU-II-79	78.8–79.3	0.5	434		Black	Op. (9%) and tr. (7%) scoria; ves. colorless g.s. (61%); felsic phenocrystals (12 %)	Opx (62%), cpx (35%)	--	--	--	See comments for T5 (short cores)	980 ± 65 AD
PU-II-106	102.3–109.8	7.5	567	1.4; 1.4; 1.4	Black	Felsics (44%), op. scoria (35%); pt scoria (13 %)	Opx (57 %), cpx (41 %)	--	--	--	TC1/2, thickest tephra in PU-II long core	1665 ± 110
PU-II-179	178.0–180.2	2.2	62	1; 1; 1	Black	Brown (48%) and colorless (32%) ves. g.s.	Opx (52 %), cpx (44%)	Alkaline andesite	--	61	TC2, 80% of ves. glass shards, differentiated suite: alkaline andesite to alkaline dacite	3240 ± 150
PU-II-255	253.8–255.8	2.0	249	2; 1; 1	Black	Brown micr. (27%) and ves. (32%) g.s.; tr. scoria (15%), felsics (15%)	Opx (61 %), cpx (35%)	Dacite	0.26	75	TC2, 59% of brownish glass shards	4110 ± 160
PU-II-377	376.8–378.1	1.3	384	2; 1.4; 1.4	Black + red	Op. (34%) and tr. scoria (34%)	Cpx (69 %), oli (23 %)	--	--	--	TC1, high cpx and olivine contents	5535 ± 140
PU-II-419	418.1–419.1	1.0	1000-1400	4; 2.9; 2.9	Black	Tr. (37%) and op. (25%) scoria; brown g.s. (25%)	Cpx (52%), opx (19%), oli (14%)	Basaltic andesite	--	41	TC1/2, coarsest tephra in PU-II long core, 2 populations of g.s.	5985 ± 125
PU-II-490	488.6–490.8	1.8	95	2.9; 2.2; 1.4	Black	Op. (34%) and tr. (29%) scoria; felsics (14%), brown g.s. (10%)	Cpx (47 %), opx (22%), oli (21%)	--	--	--	TC1/2, 21% of olivine in the heavy mineral suite	6815 ± 115
PU-II-500	497.4–502.9	5.5	411	2; 2; 1.4	Black + white	Op. (55%) and tr. scoria (20%), felsics (15%)	Cpx (53 %), opx (31 %)	--	--	--	TC1/2, relatively rich in dark brown amphibole (5%, uncommon)	6895 ± 115
PU-II-633	632.7–633.6	0.9	141	1; 1; 1	Green + gray	Colorless ves. g.s.(62%), felsics (19%)	Gg amp (56%), bg amp (19%), opx (12%)	K-rhyolite	3.57	87	62% of colorless. ves. g. s., Heavy mineralogy dominated by amp.	8455 ± 115
PU-II-744	743.5–744.5	1.0	389	1.4; 1.4; 1	Black	Tr. (35%) and op. (32%) scoria; felsics (22%)	Bg amp (24%), bb amp (15%), gg amp (6%), cpx (30%), opx (18%)	--	--	--	TC1, 15% of dark brown amphibole	10,640 ± 255
PU-II-837	836.2–837.0	0.8	192	1; 1; 1	Black	Tr. (38%) and op. (32%) scoria; felsics (19%)	Opx (56%), cpx (39%)	--	--	--	TC1/2, low content in green amphibole	12,540 ± 325
PU-II-901	899.5–903.0	3.5	154	0.7; 0.7; 0.7	Light gray	Colorless ves. g.s. (50%), felsics (35%)	Opx (76%), bg amp (13%)	Rhyolite	2.82	78	50% of colorless and highly differentiated g.s., 76% opx	13,825 ± 370
PU-II-929	928.5–929.8	1.3	190	1.4; 1; 0.7	Black	Op. (23%) and tr. (19%) scoria; brown ves. (22%) and mic. (14%) g.s; colorless ves. g.s.(12%)	Cpx (47%), opx (36%)	Andesite Rhyolite	0 3.05	50 83	TC2, Black to dark grey scoria, two geochemical populations of g.s.	14,345 ± 450
PU-II-933	932.5–933.8	1.3	365	1.4; 1.4; 1.4	Black	Tr. (41%) and op.(22%) scoria, brown mic. g.s.(15%)	Opx (64%), cpx (34%)	Andesite Rhyolite	0 3.37	51 82	TC1/2, Dark grey scoria, two geochemical populations of g.s.	14,400 ± 465
PU-II-1003	1002.4–1003.0	0.6	217	1; 0.7; 0.7	Black	Tr. (50%) and op. (32%) scoria; felsics (10 %)	Cpx (45%), oli (30%), opx (14 %)	--	--	--	TC1/2, 30% of olivine	15,510 ± 720
PU-II-1005	1005.0–1005.8	0.8	153	0.7; 0.7; 0.7	Black	Tr. (70%) and op. (14%) scoria	Cpx (37%), opx (37%)	--	--	--	TC1/2, low oli (8%) and amp (8%) contents	15,540 ± 725

Supplementary Table 3

Sample no.	SiO_2	TiO_2	Al_2O_3	FeO[a]	MgO	CaO	Na_2O	K_2O	n
Pilot cores									
PU-II-P2-4	69.62 ± 3.00	0.75 ± 0.10	14.79 ± 1.15	4.46 ± 0.73	0.87 ± 0.48	3.08 ± 1.36	3.97 ± 0.56	2.46 ± 0.75	10
PU-II-P2-8	70.45 ± 1.16	0.75 ± 0.13	14.68 ± 0.38	4.13 ± 0.37	0.72 ± 0.18	2.61 ± 0.42	3.95 ± 0.37	2.72 ± 0.20	15
PU-II-P2-11	70.48 ± 3.72	0.62 ± 0.29	15.20 ± 1.69	3.19 ± 2.27	0.59 ± 0.58	2.98 ± 0.90	4.65 ± 0.73	2.30 ± 0.77	8
PU-II-P2-11-coating	72.71 ± 2.33	0.54 ± 0.36	14.21 ± 2.46	2.78 ± 1.39	0.35 ± 0.17	2.22 ± 0.88	4.03 ± 0.66	3.15 ± 0.66	5
PU-II-P2-42	53.81 ± 0.36	1.53 ± 0.11	14.39 ± 0.39	11.39 ± 0.35	5.66 ± 0.45	9.32 ± 0.13	2.77 ± 0.20	0.89 ± 0.06	10
PU-I-P1-48	71.51 ± 0.96	0.79 ± 0.18	14.31 ± 0.34	4.20 ± 0.43	0.71 ± 0.16	2.48 ± 0.43	3.22 ± 0.18	2.78 ± 0.19	9
PU-I-P1-54	72.42 ± 4.83	0.38 ± 0.20	14.20 ± 2.20	2.98 ± 1.53	0.88 ± 0.75	2.96 ± 1.36	4.38 ± 1.02	1.81 ± 0.48	10
PU-I-P1-54-coating	74.56 ± 2.91	0.35 ± 0.18	14.38 ± 1.52	1.83 ± 0.90	0.21 ± 0.09	2.33 ± 0.70	4.39 ± 0.79	1.95 ± 0.81	6
PU-II long core									
PU-II-79	72.18 ± 0.59	0.75 ± 0.08	14.24 ± 0.15	3.97 ± 0.21	0.65 ± 0.07	2.29 ± 0.11	3.02 ± 0.25	2.91 ± 0.08	10
PU-II-179	62.10 ± 4.42	1.20 ± 0.36	16.03 ± 0.14	6.64 ± 1.81	2.45 ± 1.04	5.05 ± 1.80	4.16 ± 0.13	2.38 ± 0.60	10
PU-II-255	70.16 ± 0.77	0.89 ± 0.09	13.97 ± 0.11	5.17 ± 0.29	0.83 ± 0.07	2.68 ± 0.21	3.60 ± 0.36	2.69 ± 0.11	12
PU-II-419	56.15 ± 0.93	1.26 ± 0.23	15.13 ± 1.21	9.85 ± 0.94	4.32 ± 0.75	8.82 ± 0.40	3.58 ± 0.17	0.89 ± 0.18	9
PU-II-633	77.74 ± 0.22	0.06 ± 0.04	13.62 ± 0.16	1.32 ± 0.09	0.21 ± 0.03	1.26 ± 0.06	2.63 ± 0.23	3.17 ± 0.07	11
PU-II-901	74.75 ± 1.59	0.31 ± 0.12	14.43 ± 0.45	2.60 ± 0.55	0.57 ± 0.15	2.84 ± 0.58	2.81 ± 0.29	1.69 ± 0.50	11
PU-II-929-pop 1	73.85 ± 0.56	0.37 ± 0.08	14.91 ± 0.19	2.48 ± 0.14	0.40 ± 0.08	1.71 ± 0.19	3.49 ± 0.15	2.78 ± 0.10	9
PU-II-929-pop 2	58.86 ± 0.80	1.72 ± 0.17	15.24 ± 0.08	9.25 ± 0.34	3.04 ±0.35	6.74 ± 0.33	3.81 ± 0.16	1.36 ± 0.13	3
PU-II-933-pop 1	59.47 ± 1.24	1.86 ± 0.08	14.88 ± 0.40	9.46 ± 0.46	2.84 ± 0.55	6.42 ± 0.65	3.55 ± 0.54	1.51 ± 0.23	5
PU-II-933-pop 2	67.24 ± 0.00	0.89 ± 0.00	14.94 ± 0.00	5.76 ± 0.00	1.06 ± 0.00	3.76 ± 0.00	3.42 ± 0.00	2.93 ± 0.00	1
PU-II-933-pop 3	73.50 ± 1.66	0.39 ± 0.19	15.48 ± 1.56	2.25 ± 0.52	0.37 ± 0.18	1.92 ± 0.56	3.57 ± 1.03	2.53 ± 0.56	5
Historical lavas[b]									
CC-1960	70.38 ± 0.31	0.69 ± 0.02	14.27 ± 0.04	4.06 ± 0.07	0.47 ± 0.07	2.19 ± 0.07	5.17 ± 0.20	2.78 ± 0.04	7
CC-1921-22	69.47 ± 0.11	0.78 ± 0.03	14.47 ± 0.06	4.37 ± 0.10	0.63 ± 0.06	2.50 ± 0.07	5.15 ± 0.13	2.63 ± 0.01	4

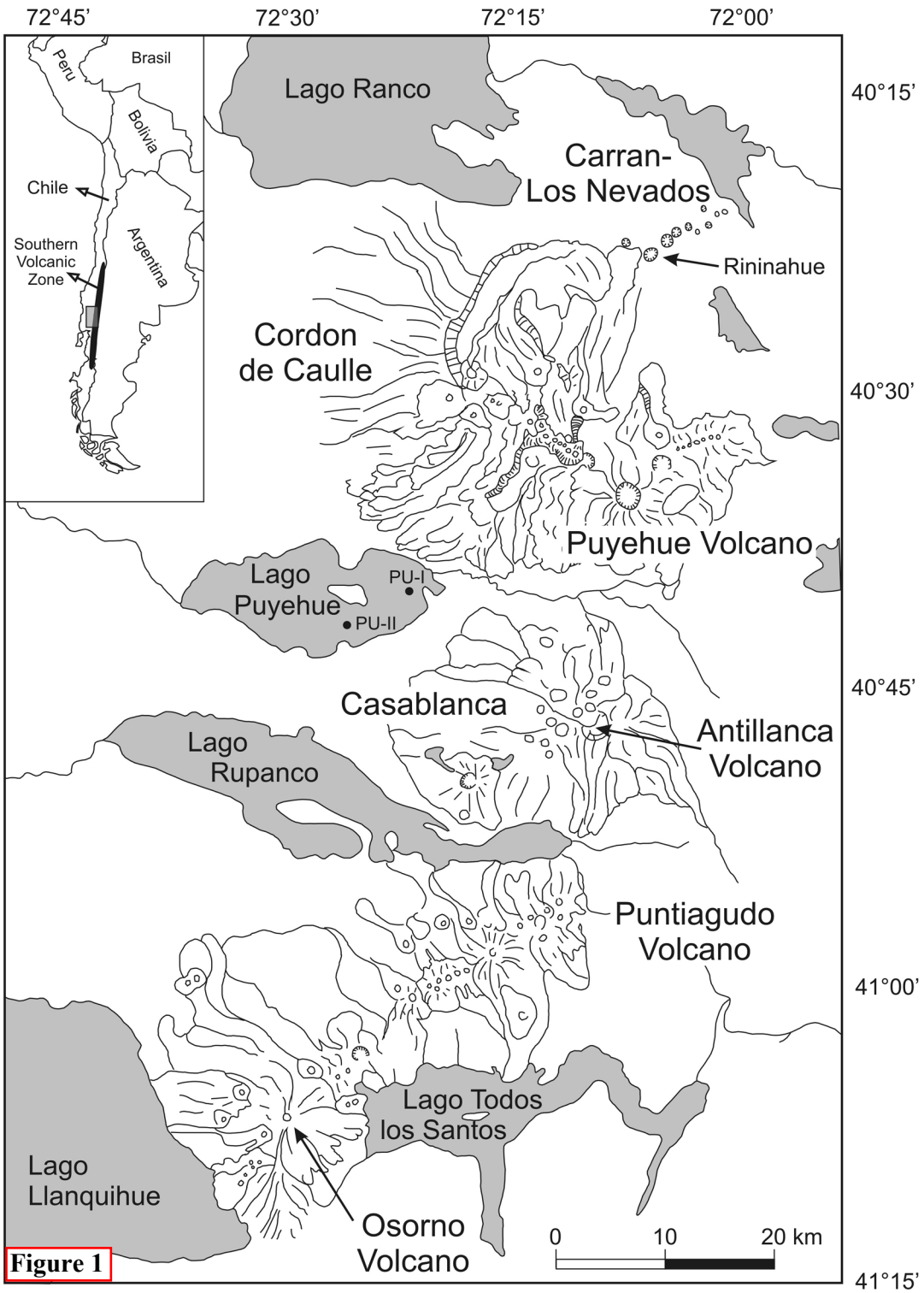
72°45'
72°30'
72°15'
72°00'
40°15'
40°30'
40°45'
41°00'
41°15'
Peru
Brasil
Bolivia
Chile
Argentina
Southern Volcanic Zone
Lago Ranco
Carran-Los Nevados
Rininahue
Cordon de Caulle
Puyehue Volcano
Lago Puyehue
PU-I
PU-II
Casablanca
Antillanca Volcano
Lago Rupanco
Puntiagudo Volcano
Lago Todos los Santos
Lago Llanquihue
Osorno Volcano
0
10
20 km

Figure 1

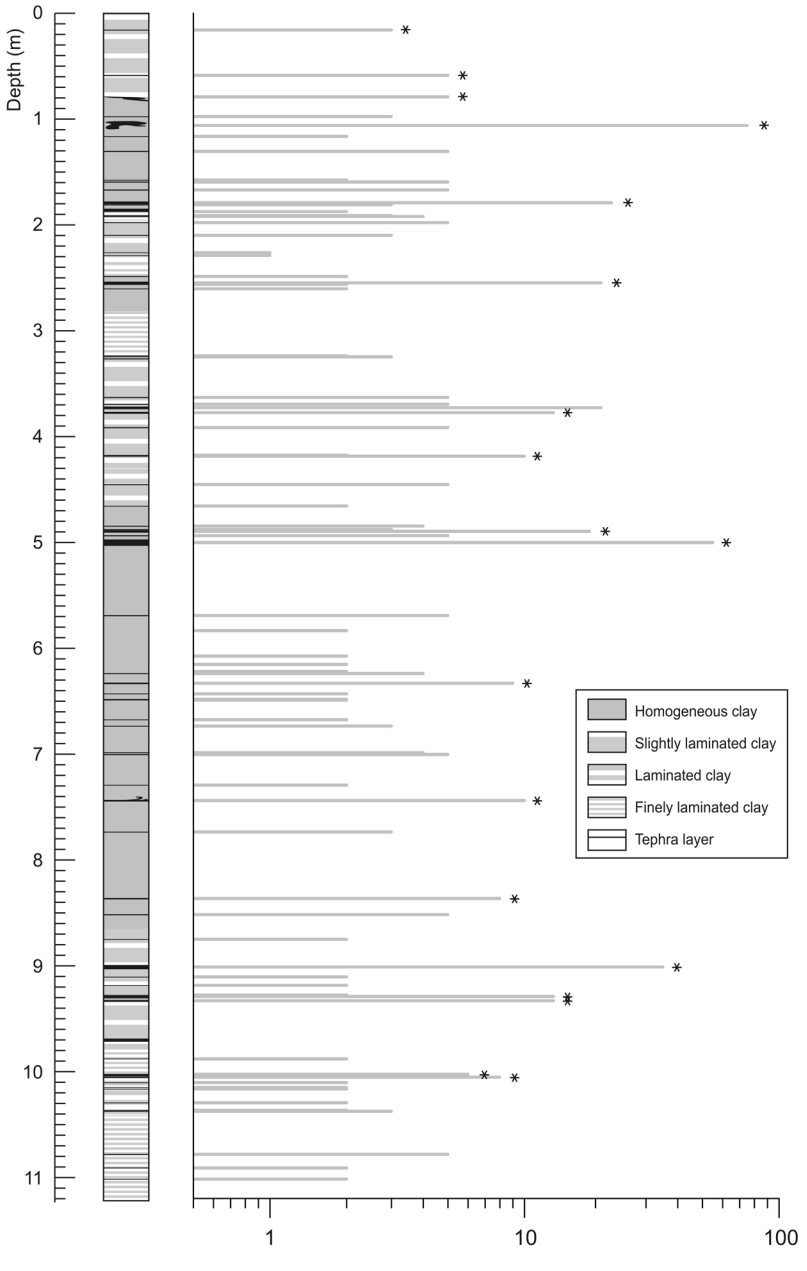
Depth (m)
0
1
2
3
4
5
6
7
8
9
10
11
Homogeneous clay
Slightly laminated clay
Laminated clay
Finely laminated clay
Tephra layer
1
10
100
Tephra thickness (mm)- Logarithmic scale

Figure 2

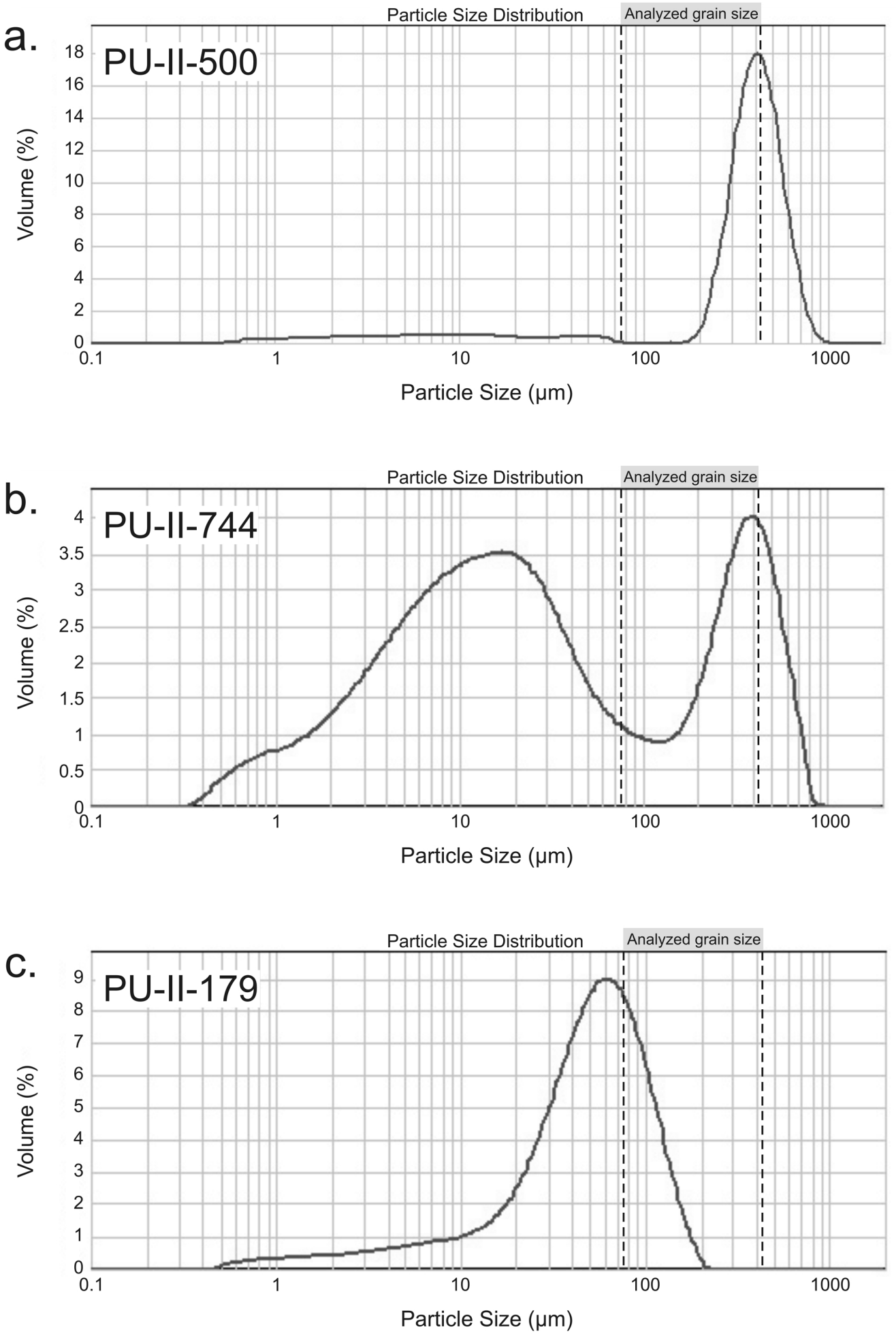
a.
PU-II-500
Particle Size Distribution
Analyzed grain size
Volume (%)
Particle Size (μm)
b.
PU-II-744
Particle Size Distribution
Analyzed grain size
Volume (%)
Particle Size (μm)
c.
PU-II-179
Particle Size Distribution
Analyzed grain size
Volume (%)
Particle Size (μm)

Figure 3

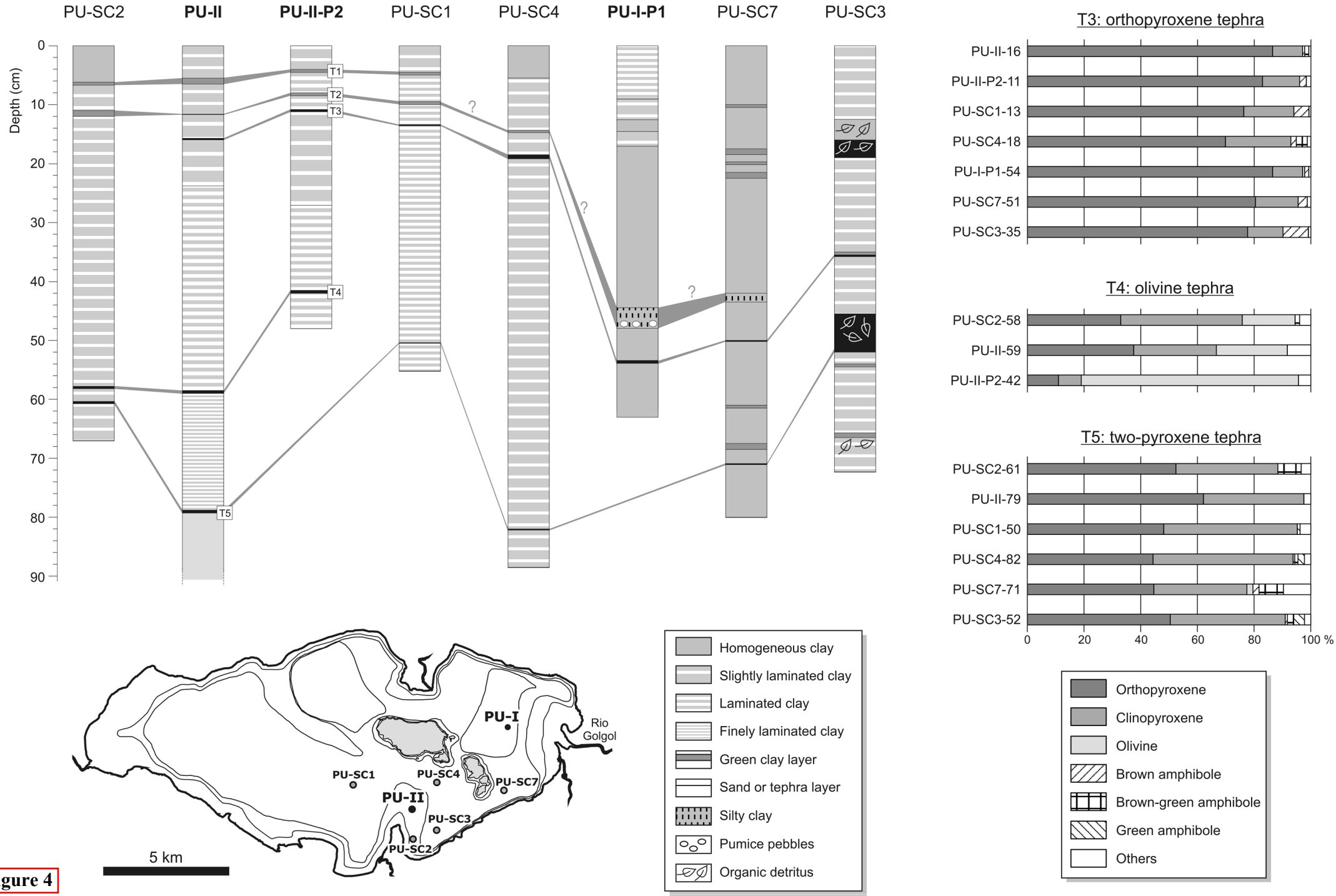
PU-SC2
PU-II
PU-II-P2
PU-SC1
PU-SC4
PU-I-P1
PU-SC7
PU-SC3
Depth (cm)
0
10
20
30
40
50
60
70
80
90
T1
T2
T3
T4
T5
?
?
?
T3: orthopyroxene tephra
PU-II-16
PU-II-P2-11
PU-SC1-13
PU-SC4-18
PU-I-P1-54
PU-SC7-51
PU-SC3-35
T4: olivine tephra
PU-SC2-58
PU-II-59
PU-II-P2-42
T5: two-pyroxene tephra
PU-SC2-61
PU-II-79
PU-SC1-50
PU-SC4-82
PU-SC7-71
PU-SC3-52
0
20
40
60
80
100 %
PU-I
Rio Golgol
PU-SC1
PU-SC4
PU-SC7
PU-II
PU-SC3
PU-SC2
5 km
Homogeneous clay
Slightly laminated clay
Laminated clay
Finely laminated clay
Green clay layer
Sand or tephra layer
Silty clay
Pumice pebbles
Organic detritus
Orthopyroxene
Clinopyroxene
Olivine
Brown amphibole
Brown-green amphibole
Green amphibole
Others

Figure 4

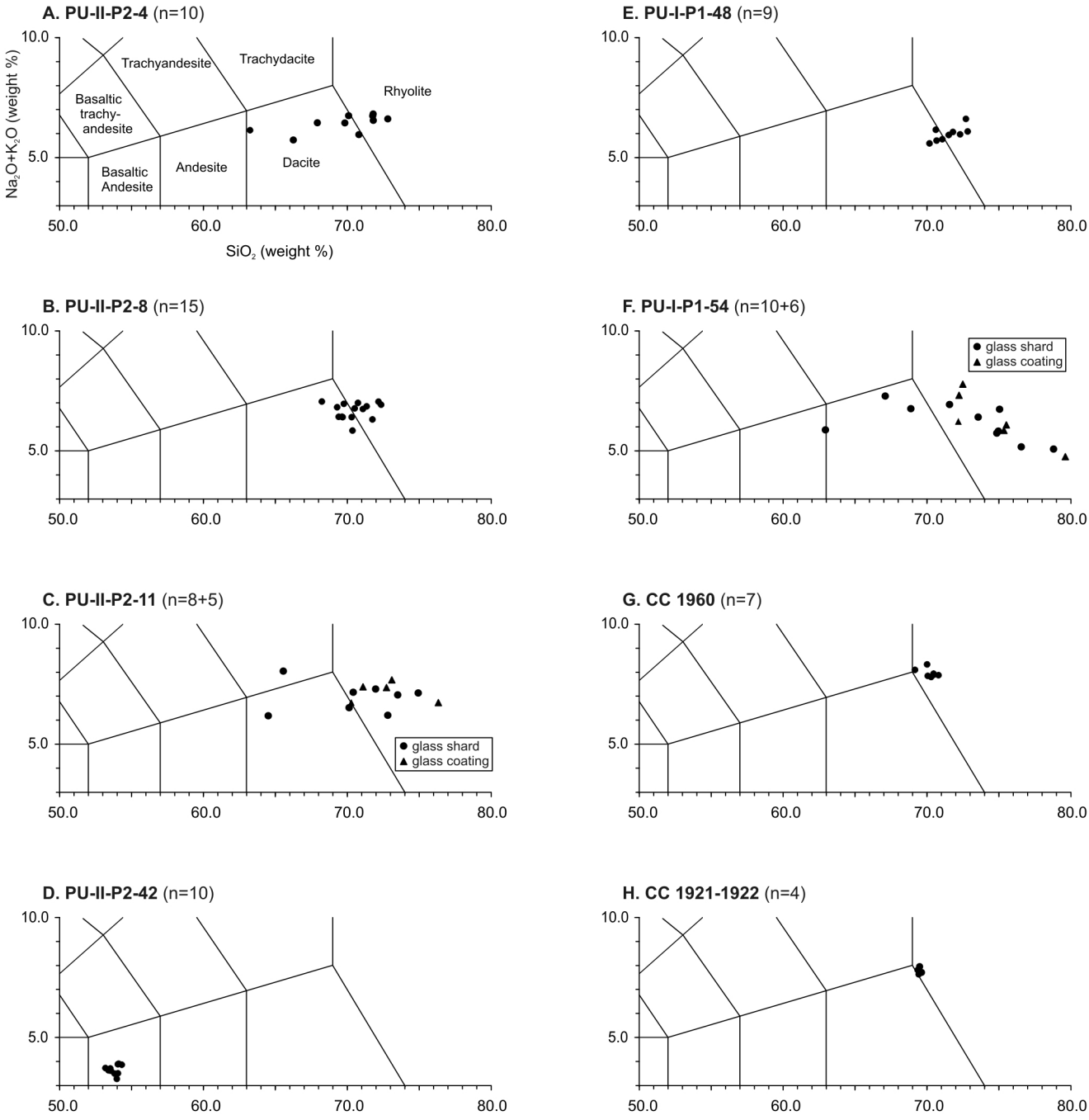
A. PU-II-P2-4 (n=10)
B. PU-II-P2-8 (n=15)
C. PU-II-P2-11 (n=8+5)
D. PU-II-P2-42 (n=10)
E. PU-I-P1-48 (n=9)
F. PU-I-P1-54 (n=10+6)
G. CC 1960 (n=7)
H. CC 1921-1922 (n=4)
Trachyandesite
Trachydacite
Rhyolite
Basaltic trachy-andesite
Basaltic Andesite
Andesite
Dacite
glass shard
glass coating
10.0
5.0
50.0
60.0
70.0
80.0
Na2O+K2O (weight %)
SiO2 (weight %)

Figure 5

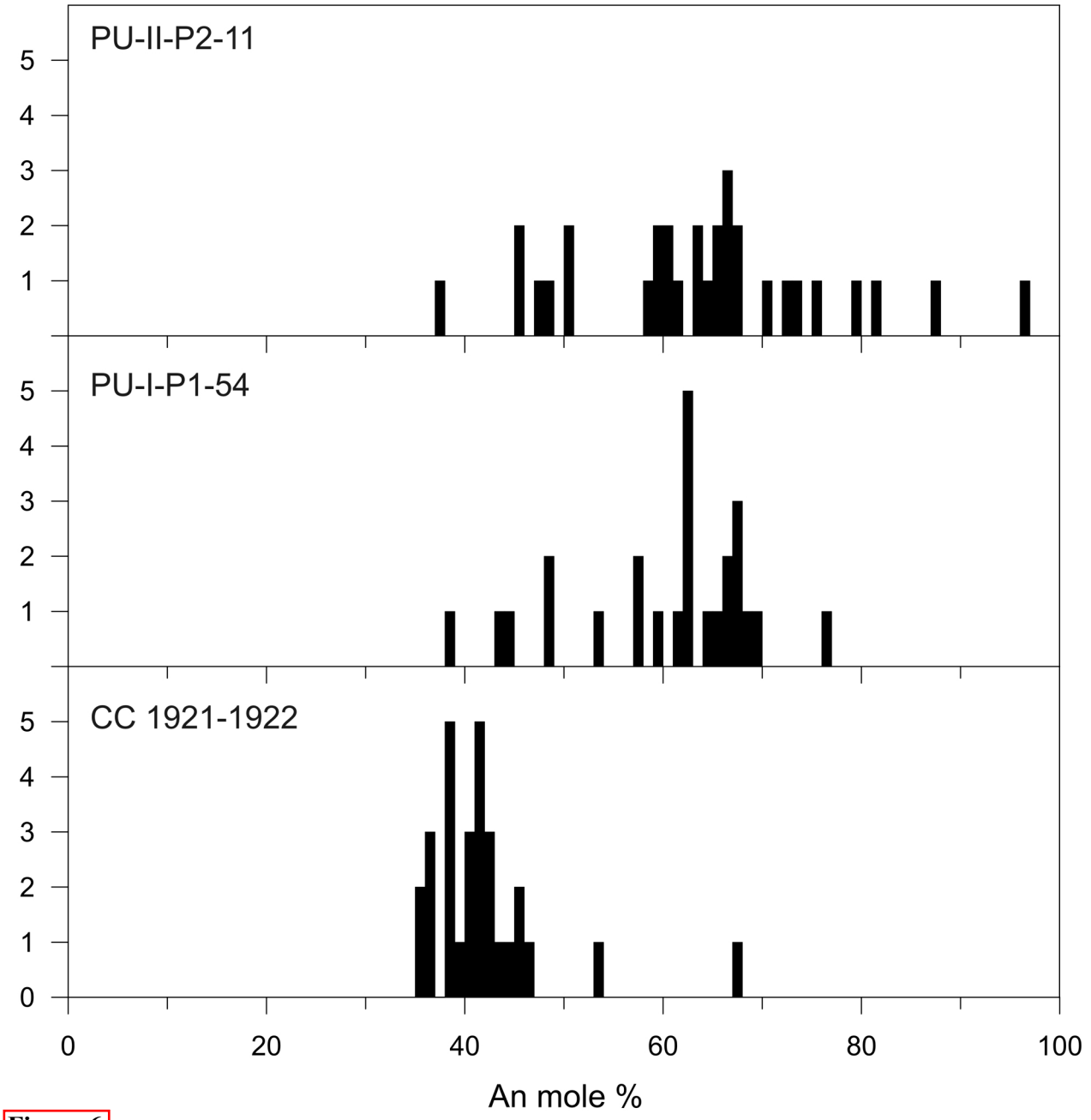

Figure 6

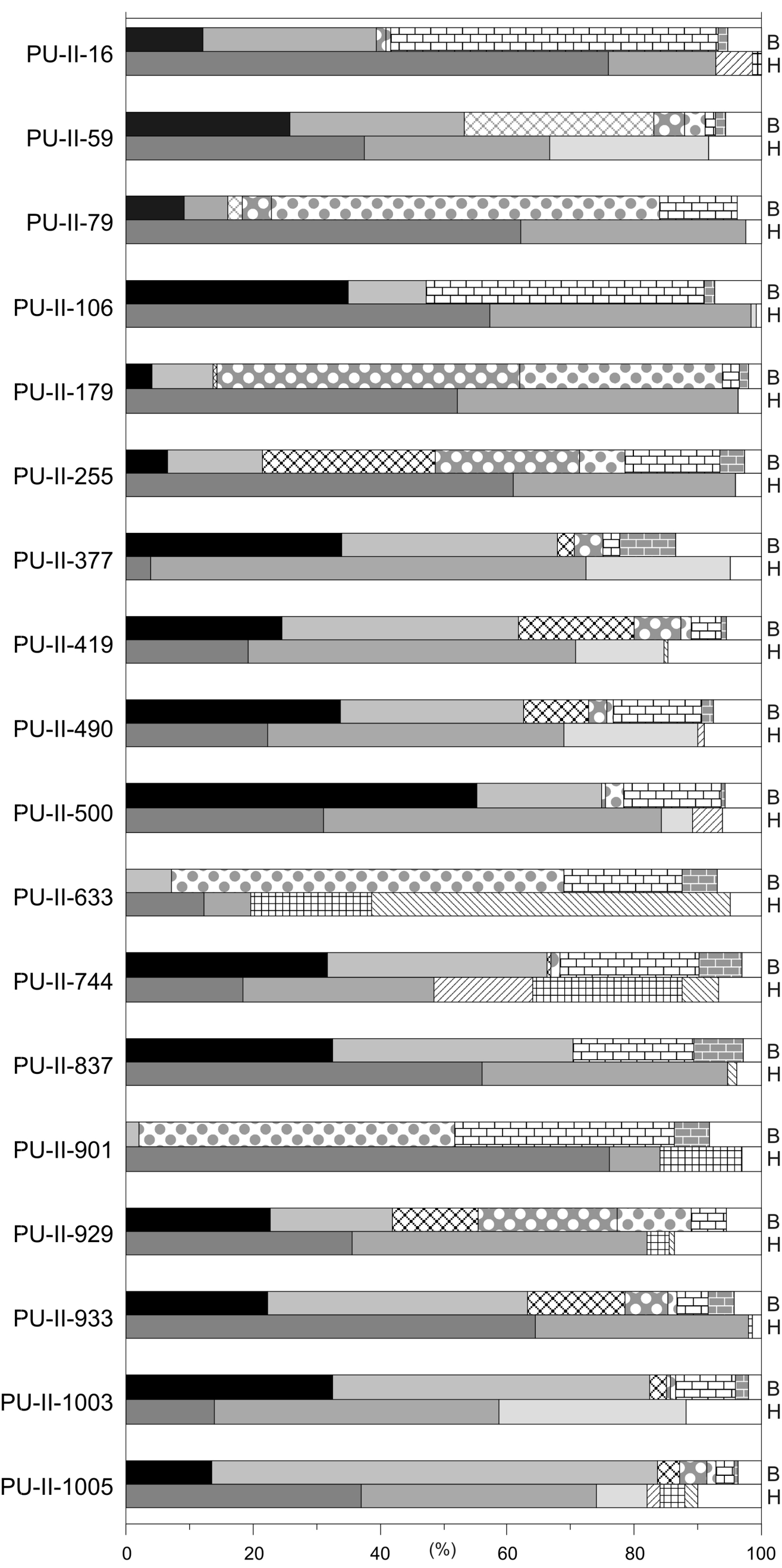
PU-II-16
PU-II-59
PU-II-79
PU-II-106
PU-II-179
PU-II-255
PU-II-377
PU-II-419
PU-II-490
PU-II-500
PU-II-633
PU-II-744
PU-II-837
PU-II-901
PU-II-929
PU-II-933
PU-II-1003
PU-II-1005
B
H
0
20
40
(%)
60
80
100
Bulk mineralogy (B)
Opaque scoriae
Translucent scoriae
Massive or microscrystalline brown glass shards
Vesiculated brown glass shards
Vesiculated colorless glass shards
Felsic phenocrystals
Mafic phenocrystals
Others
Heavy mineralogy (H)
Orthopyroxene
Clinopyroxene
Olivine
Brown amphibole
Brown-green amphibole
Green amphibole
Others

Figure 7

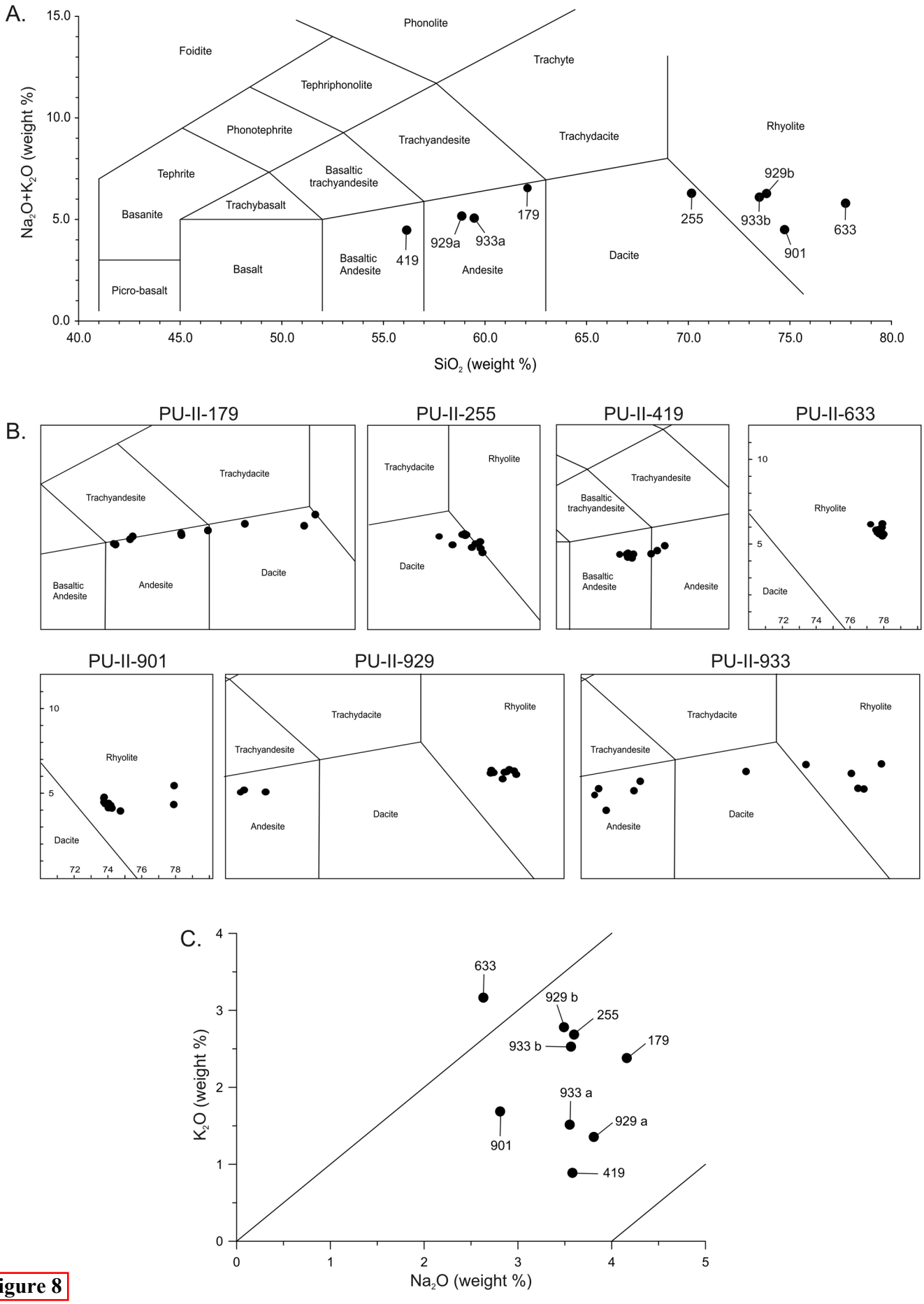
A.
Phonolite
Foidite
Trachyte
Tephriphonolite
Phonotephrite
Trachyandesite
Trachydacite
Rhyolite
Tephrite
Basaltic trachyandesite
Trachybasalt
Basanite
Basalt
Basaltic Andesite
Andesite
Dacite
Picro-basalt
929b
933b
633
255
179
929a
933a
419
901
Na2O+K2O (weight %)
SiO2 (weight %)
B.
PU-II-179
PU-II-255
PU-II-419
PU-II-633
PU-II-901
PU-II-929
PU-II-933
Trachydacite
Trachyandesite
Basaltic Andesite
Andesite
Dacite
Rhyolite
Basaltic trachyandesite
C.
K2O (weight %)
Na2O (weight %)

Figure 8